Renewable and Sustainable Energy Reviews 41 (2015) 715–734

Contents lists available at ScienceDirect

Renewable and Sustainable Energy Reviews

journal homepage: www.elsevier.com/locate/rser

Review of convection heat transfer and fluid flow in porous media with nanofluid

Raed Abed Mahdi [a,b,c,*], H.A. Mohammed [c,**], K.M. Munisamy [a], N.H. Saeid [d]

[a] Department of Mechanical Engineering, College of Engineering, Universiti Tenaga Nasional, Jalan IKRAM-UNITEN, 43000 Kajang, Selangor, Malaysia
[b] Department of Mechanical Maintenance, Doura Power Station, Ministry of Electricity, 10022 Al-doura quarter, Almahdia place, Baghdad, Iraq
[c] Department of Thermo fluids, Faculty of Mechanical Engineering, Universiti Teknologi Malaysia, 81310 UTM Skudai, Johor Bahru, Malaysia
[d] Department of Mechanical Engineering, Institute of Teknologi Brunei, Jalan Tungku Link, Gadong BE 1410, Brunei Darussalam

ARTICLE INFO

Article history:
Received 8 April 2013
Received in revised form
29 April 2014
Accepted 17 August 2014

Keywords:
Nanofluids
Porous media
Effective thermal conductivity
Effective viscosity
Porosity
Permeability
Inertia coefficient

ABSTRACT

There are two advantages of using porous media. First, its dissipation area is greater than the conventional fins that enhances the heat convection. Second is the irregular motion of the fluid flow around the individual beads which mixes the fluid more effectively. Nanofluids result from the mixtures of base fluid with nanoparticles having dimensions of (1–100) nm, with very high thermal conductivities; as a result, it would be the best convection heat transfer by using two applications together: porous media and nanofluids. This article aims to summarize the published articles in respect to porosity, permeability (K) and inertia coefficient (C_f) and effective thermal conductivity (k_{eff}) for porous media, also on the thermophysical properties of nanofluid and the studies on convection heat transfer in porous media with nanofluid.

Contents

* Corresponding author at: Department of Thermo fluids, Faculty of Mechanical Engineering, Universiti Teknologi Malaysia, 81310 UTM Skudai, Johor Bahru, Malaysia. Tel.: +60 7 55 34716; fax: +60 7 55 66 159.
** Corresponding author.
E-mail addresses: eng_raed_2005@yahoo.com (R.A. Mahdi), hussein.dash@yahoo.com (H.A. Mohammed).

http://dx.doi.org/10.1016/j.rser.2014.08.040
1364-0321/

Nomenclature

A	cross section area (m^2)
C	shape factor ≈ 150 (Blake–Kozeny), 180 (Carman–Kozeny)
Cf	Forchheimer coefficient
Cp	specific heat capacity, (J/kg K)
Da	Darcy number
D_h	hydraulic diameter, (m)
D_p	mean particle diameter, (m)
Gr	Grashof number
h	heat transfer coefficient, (W/m^2 K)
K	permeability for porous media, (m^2)
k	thermal conductivity, (W/mK)
Le	Lewis number
M	molecular weight of the base fluid
N	Avogadro number
Nu	Nusselt number
Pe	Péclet number
Pr	Prandtl number
Ra	Rayleigh number
Re	Reynolds number
Ri	Richardson number
Sh	Sherwood number
V	volume

Greek symbols

Δp	pressure drop
ε	porosity
μ	dynamic viscosity, (kg/ms)
ρ	density, (kg/m^3)
ρ_{fo}	mass density of the base fluid calculated at temperature $T=293^\circ$ K
α	thermal diffusivity, (m^2/s)
φ	nanoparticle volume fraction

Subscripts

b	base fluid
f	fluid
nf	nanofluid
p	particle
r	radial direction
s	solid
eff	effective
$p.m$	porous media

1. Introduction

In thermal devices, improvement of convection heat transfer becomes an important factor in industries like electronic equipment and heat exchangers. Heat exchangers may be classified according to transfer process, construction, flow arrangement, surface compactness, number of fluids, and heat transfer mechanisms as shown in Fig. 1. Some of these classifications have been dealt in [1–8].

In industrial processes, another method for improving the convection heat transfer characteristics is using porous medium (any material which consists of solid matrix with an interconnected void is called porous media such as rocks and open-cell aluminum foams [9]) and nanofluid. Therefore, porous media technique has been the subject of many studies and has received a considerable observation. This attention is due to the fact that this kind of structure is encountered in many engineering applications, such as filtration, thermal insulation, ground water, oil flow and all types of heat exchangers.

Convection heat transfer and fluid flow with porous medium occur in power stations of many engineering applications where cooling or heating is required such as cooling turbine blades, cooling electronic equipment and combustion systems. The mixing of the low and high energy fluids which occur in these applications significantly affects the performance of these devices [10]. One of the ways to increase heat transfer is to employ porous medium with nanofluid.

2. Fluid flow in porous media

Fluid flow through a porous medium depends on Darcy's law (1856), where fluid flow discharge rate in the porous media is proportional to the pressure drop and the viscosity of the fluid over a given distance [11] as shown in Fig. 2.

$$\nabla p = -\frac{\mu}{K}\vec{v} \tag{1}$$

Darcy's law was later found to be limited in accuracy and only valid for low velocity flows that are incompressible and isothermal. Further research brought forth the Dupuit–Forchheimer extension to Darcy's law which is represented in Eq. (2). This addition to Darcy's law defines the form drags effect on the flow, which is represented by the inertial resistance coefficient (C_f). The relationship of inertial resistance is non-linear and affects higher velocity flows, but it varies with respect to pore size, internal structure, and porosity [9].

$$-\nabla p = \underbrace{\frac{\mu}{K}\vec{v}}_{\text{Darcy term}} + \underbrace{\frac{\rho c_f}{\sqrt{K}}|v|v_j}_{\text{Forchheimer term}} \tag{2}$$

where C_f is the Forchheimer coefficient (inertia coefficient).

Flows in porous media are defined as being in one of three ranges, which are determined from the Reynolds number of the flow. They are laminar, non-linear laminar (the transition between the Darcy regime, where viscous effects dominate, to the Forchheimer regime, where inertial effects dominate) and turbulent ranges [9]. Several methods for calculating the Reynolds number for flows in porous media have been proposed. Oosthuizen et al. [12] and Boomsma and Poulikakos [13] used square root of permeability to calculate the Reynolds number value in porous medium as show in Eq. (3); this use is best acceptable with low porous medium porosity. Non-linear laminar flow occurs in the Re_K range 1–10 [9]. For this relation and condition, Bonnet et al. [14] elaborated that it was valid for laminar flow only. Boomsma and Poulikakos [15] and Bonnet et al. [14] used mean pore diameter to calculate the Reynolds number in porous medium as show in Eq. (4). Using the pore size as the length scale has been found to be more accurate, since permeability and inertial resistance are dependent on pore size [16].

$$Re_K = \frac{\rho u\sqrt{K}}{\mu} \tag{3}$$

$$Re_{D_p} = \frac{\rho u D_p}{\mu} \tag{4}$$

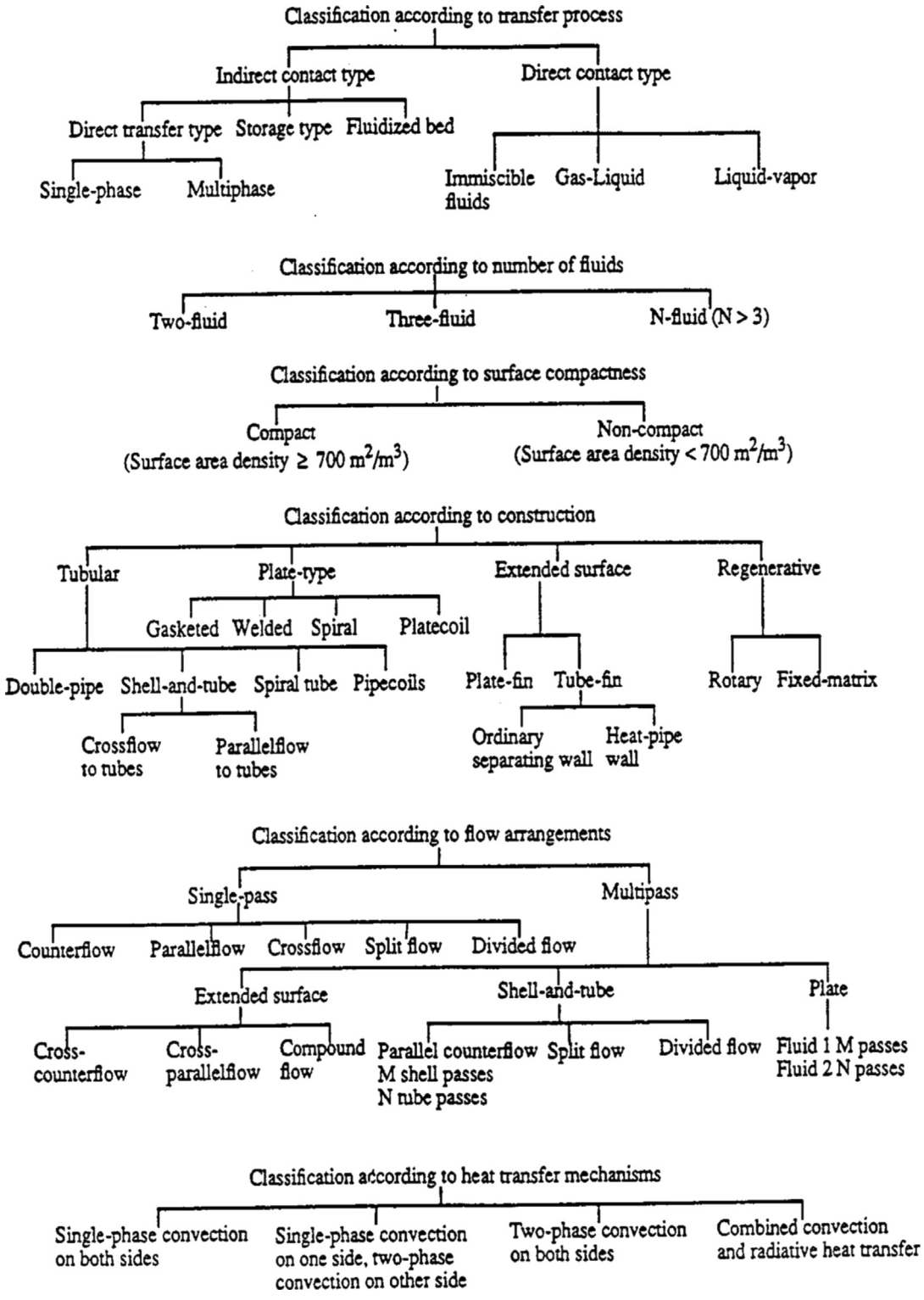

Fig. 1. Classification of heat exchangers [1].

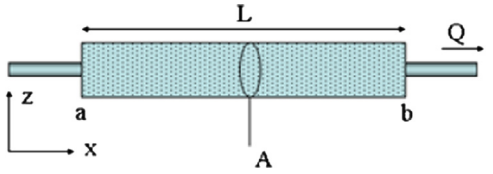

Fig. 2. Diagram showing definitions and directions for Darcy's law [11].

Darcy velocity is defined as the fluid velocity inside the porous media ($u_{p.m}$) and is related to the physical velocity $u(y)$ (the actual fluid velocity outside the porous region) as shown in Eq. (5) and Fig. 3 [17]:

$$u_{Darcy} = \varepsilon u_{physical} \tag{5}$$

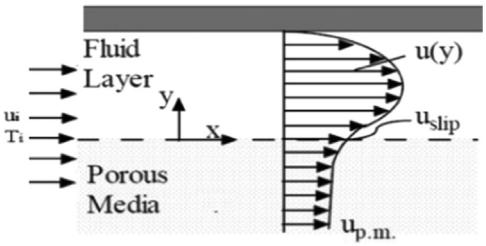

Fig. 3. Darcy velocity in porous media [17].

3. Porous media characteristics

In this section, the porosity (ε), permeability (K) and inertia coefficient (C_f) and thermal conductivity (k_{eff}) for porous media are discussed.

3.1. Porosity (ε)

Nield and Bejan [9] defined the pores as voids which allow the fluids to flow through the material. The porosity (ε) is the total

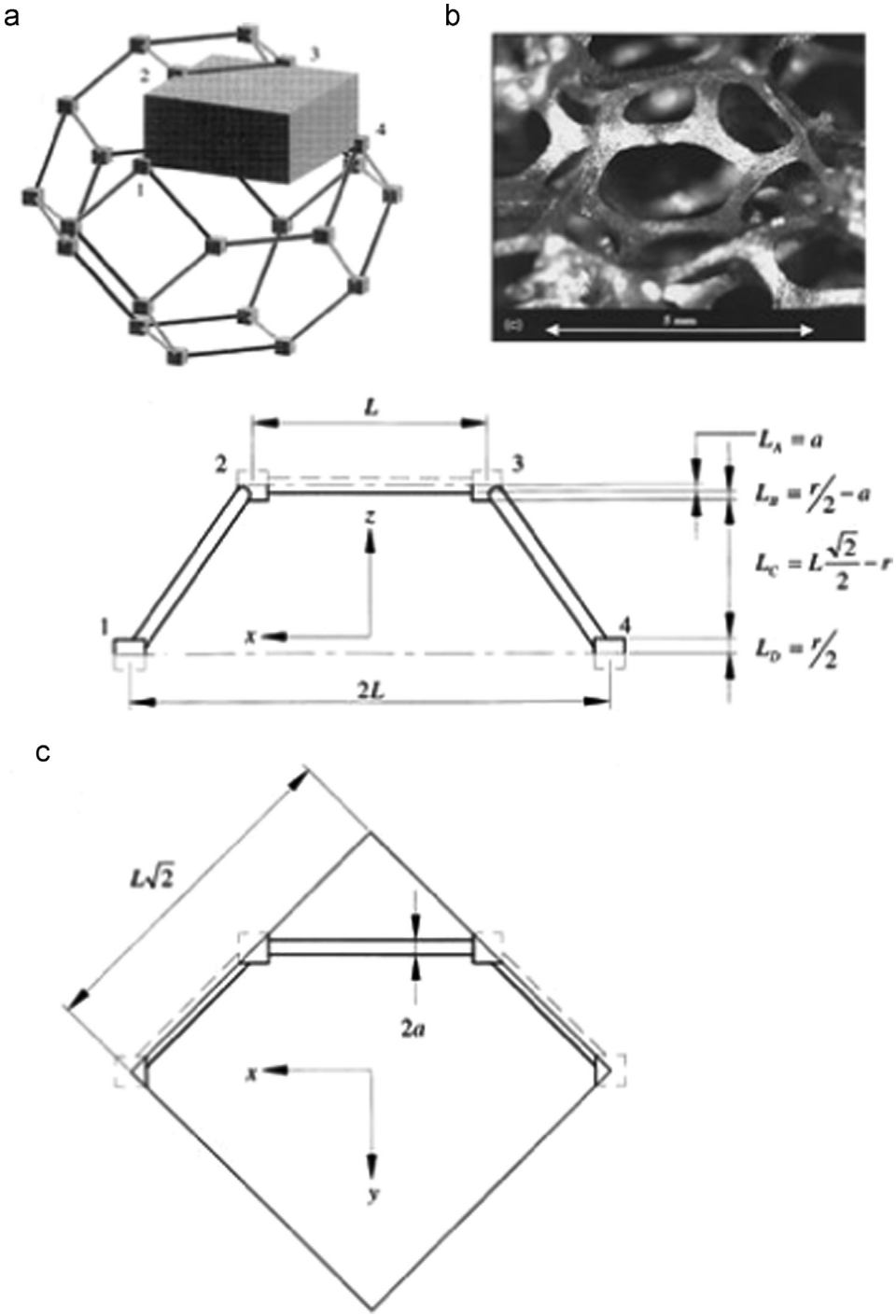

Fig. 4. (a) The tetrakaidecahedron model, (b) single tetrakaidecahedron cell in aluminum foam and (c) the geometrical breakdown of the tetrakaidecahedron unit cell [13].

voids volume to the total porous media volume. For that, Jiang et al. [18] computed each run according to the following definition:

$$\varepsilon = \frac{V_{void}}{V_{solid}} = 1 - \frac{V_{solid}}{V_{total}} \tag{6}$$

Fu et al. [19] defined the porosity in **porous block** which was made of **spherical beads** as shown in the following equation:

$$\varepsilon = \varepsilon_e[1 + r_1 e^{-r_2 \Delta s/d_p}] \tag{7}$$

where Δs is the short distances from the boundaries of the porous block to the calculated point [m], d_p is the particle diameter [m], ε_e is the effective porosity and r_1, r_2 are the coefficients.

The porosity of the **aluminum foams** was calculated analytically by Boomsma and Poulikakos [13] where they took the cells in their connected state; based on symmetry, a representative section was selected. One-sixteenth of a single tetrakaidecahedron cell was encapsulated, as shown in Fig. 4. This presented a section which contained all the geometrical characteristics relating to the tetrakaidecahedron.

$$\varepsilon = 1 - \frac{\sqrt{2}}{2}\left[de^2 + \frac{1}{2}\pi d^2(1-e) + \left(\frac{1}{2}e - d\right)e^2 + \pi d^2(1-2e^{\sqrt{2}}) + \frac{1}{4}e^3\right] \tag{8}$$

where d is the dimensionless foam ligament radius and e is the dimensionless cubic node length.

Boomsma et al. [20] used compression factor (M) and the uncompressed porosity (manufacturer's stated initial porosity) to calculate compressed porosity of the **aluminum foams** as shown in Fig. 5; the relationship was represented graphically.

$$\varepsilon_{compressed} = 1 - M(1 - \varepsilon_{uncompressed}) \tag{9}$$

Jiang et al. [21] computed porosities of the **sintered porous** plates depending on the weight of sintered porous plate and its dimension:

$$\varepsilon = 1 - \frac{M_t - \rho_c \sigma_c w_p L}{\rho_p(\sigma_t - \sigma_c) w_p L} \tag{10}$$

where M is the sintered porous plate weight, w_p is the sintered porous plate width, L is the channel length, σ is the thickness, c is the copper and t is the total.

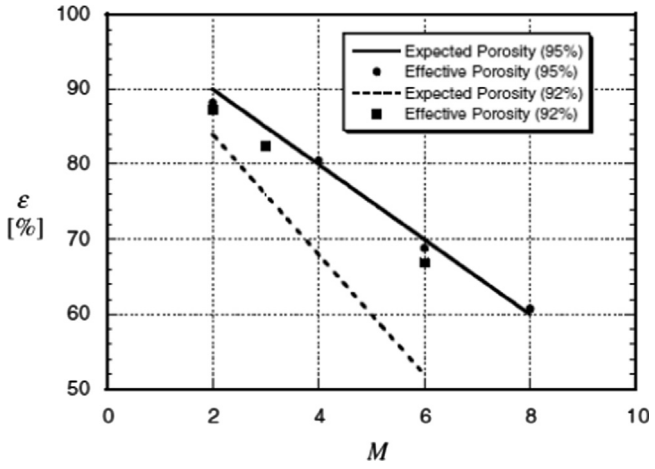

Fig. 5. Plot of the porosity of the raw foam material which was used in the aluminum foam heat exchangers. The lines denote the porosity predicted by the manufacturer's stated initial porosity (ε) and compression factor (M) based on Eq. (9), while the individual points are the measured values for the raw foam material [20].

3.2. Permeability (K) and inertia coefficient (C_f)

Permeability is defined as the surface area that is open to flow, and it depends on the porous medium nature and the fluid properties [22]. Caudle [23] and Kleinstreuer [17] defined that the permeability (K) of porous media is a term used to express the area through its fluid flow in porous media cross section and its unit is area unit [m^2].

There are some methods for calculating the permeability and the inertia coefficient through analytical and experimental methods which are summarized as follows.

Calmidi [24] gave specific formulations for (K) and (C_f) based on experimental data [25]. Calmidi [24] proposed an open-cell **metal foam** representation, as shown in Fig. 6 [16], to approximate the

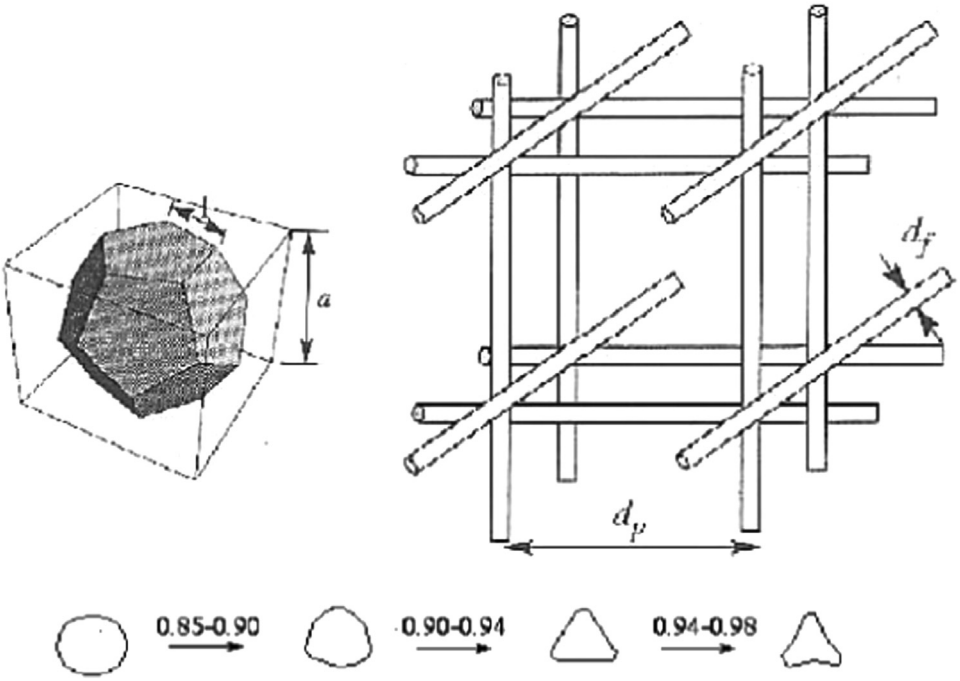

Fig. 6. Open cell representation of metal foam and schematics of the fiber cross sections at different porosities [25].

metal foam structure. It is shaped as a cube of unit volume.

$$K = 0.00073 d_p^2 (1-\varepsilon)^{-0.224} \left(\frac{d_f}{d_p}\right)^{-1.11} \tag{11}$$

$$c_f = 0.00212(1-\varepsilon)^{-0.132} \left(\frac{d_f}{d_p}\right)^{-1.63} / \sqrt{K} \tag{12}$$

$$\frac{d_f}{d_p} = 1.18\sqrt{\frac{1-\varepsilon}{3\pi}} \times \frac{1}{G} \tag{13}$$

$$G \text{ is a shape function} = 1 - e^{((-1-\varepsilon)/0.04)} \tag{14}$$

Calmidi [24] found Eq. (13) to match the measurement of d_f and d_p within $\pm 7\%$ [16]. Bhattacharya et al. [16] and Plessis et al. [26] derived permeability (K) and inertial coefficient models by using experimental results from **foam samples** of very small pore sizes (45–100PPI) and porosity of 0.973–0.978, and using water and glycerol as the fluid phases. Their expression for permeability (K) was represented as

$$K = \frac{(\sqrt{\chi/(3\varepsilon)}d_p)^2 \varepsilon^2}{36\chi(\chi-1)} \tag{15}$$

$$\frac{1}{\chi} = \frac{\pi}{4\varepsilon}\left\{1 - \left(1.18\sqrt{\frac{(1-\varepsilon)}{3\pi}} \times \frac{1}{G}\right)^2\right\} \tag{16}$$

where χ is the tortuosity of the porous matrix; it is defined as the ratio of the representative unit cell of the porous medium to the basic stream-wise length scale, and G is the geometric function.

Their expression for the inertial coefficient was represented by

$$c_f = 0.095\frac{C_D}{12} G^{-0.8} \sqrt{\frac{\varepsilon}{3(\chi-1)}} \left(1.18\sqrt{\frac{(1-\varepsilon)1}{3\pi \quad G}}\right)^{-1} \tag{17}$$

where C_D is the form drag coefficient.

Jiang and Lu [27] studied the **sintered bronze porous** (the particles were spherical) plate channels, convection heat transfer and fluid flow of water and used Ergun's equations [9,28] to calculate the permeability (K) and inertial coefficient values.

$$K = \frac{d_p^2 \varepsilon^3}{150(1-\varepsilon)^2} \quad \text{(Blake} - \text{Kozony's equation [9])} \tag{18}$$

$$c_f = \frac{1.75}{\sqrt{150}\varepsilon^{1.5}} \tag{19}$$

Nebbali and Bouhadef [29] studied numerically the heat transfer enhancement in a parallel-plate channel by using **porous blocks**. Porous blocks were inserted to partially fill the channel. They used the modified permeability in the momentum equations for non-Newtonian fluids which relies on the porous media structure and it was given by Christopher and Middleman [30].

$$K^* = \frac{1}{2Ct}\left(\frac{n\varepsilon}{3n+1}\right)^n \left(\frac{50K}{3\varepsilon}\right)^{(n+1)/2} \tag{20}$$

where (K) is the intrinsic permeability and (Ct) is the tortuosity factor.

There are various methods to calculate the permeability and the inertia coefficient experimentally. One of these methods was adopted by Givler and Altobelli [31] who linearized the Darcy–Forchheimer equation in their experiments and plotted the pressure drop versus the velocity to obtain the (K) and (C_f) [15]. Consequently, Jiang and Lu [27] used this method to compare the values of permeability and the inertia coefficient from the numerical results and those calculated using correlations (17) and (18) for three particle diameters.

Darcy–Forchheimer equation can be rearranged as follows:

$$\left[\frac{\Delta p}{L}\right]_{\text{exp.}} = \frac{\mu}{K}u + \frac{\rho c_f}{\sqrt{K}}u^2 \tag{21}$$

$$\left[\frac{\Delta p}{L}\right]_{\text{exp.}} \times \frac{1}{u} = \frac{\mu}{K} + \frac{\rho c_f}{\sqrt{K}}u = A + mX \tag{22}$$

$$K = \frac{\mu}{A} \tag{23}$$

$$c_f = \frac{m\sqrt{K}}{\rho} \tag{24}$$

Permeability (K) and inertia coefficient (C_f) can be calculated depending on the pressure drop and the velocity. It can be extrapolated from the form of pressure drop versus velocity data through the porous component to determine the permeability (K) and inertia coefficient (C_f) [32].

$$\left[\frac{\Delta p}{L}\right]_{\text{exp.}} = \frac{\mu}{K}u + \frac{\rho c_f}{\sqrt{K}}u^2 \tag{25}$$

$$\Delta p = au + bu^2 \tag{26}$$

$$a = \frac{\mu L}{K} \Rightarrow K = \frac{\mu L}{a} \tag{27}$$

$$b = \frac{\rho c_f L}{\sqrt{K}} \Rightarrow c_f = \frac{b\sqrt{K}}{\rho L} \tag{28}$$

The least square curve fitting method was used by Bhattacharya et al. [16], Antohe and Lage [33] and Boomsma and Poulikakos [15] as another method to calculate the permeability and the inertia coefficient through the pressure drop versus velocity data points plotted. Eq. (2) can be rearranged as follows:

$$\left[\frac{\Delta p}{L}\right]_{\text{exp.}} = \frac{\mu}{K}u + \frac{\varepsilon\rho c_f}{\sqrt{K}}u^2 \tag{29}$$

$$[\Delta p]_{\text{exp.}} = Au + Bu^2 \tag{30}$$

$$A = \frac{\mu}{K} \tag{31}$$

$$B = \frac{\rho c_f}{\sqrt{K}} \tag{32}$$

By using numerical methods, the coefficients A and B in Eq. (29) are solved using one of curve fitting techniques. Applying the least square curve fit (the better line has minimum error between line and data points) to the above equation gives the following results for coefficients A and B:

$$A = \frac{(\Sigma_{i=1}^n x_i y_i)(\Sigma_{i=1}^n x_i^4) - (\Sigma_{i=1}^n x_i^2 y_i)(\Sigma_{i=1}^n x_i^3)}{(\Sigma_{i=1}^n x_i^2)(\Sigma_{i=1}^n x_i^4) - (\Sigma_{i=1}^n x_i^3)(\Sigma_{i=1}^n x_i^3)} \tag{33}$$

$$B = \frac{(\Sigma_{i=1}^n x_i^2 y_i)(\Sigma_{i=1}^n x_i^2) - (\Sigma_{i=1}^n x_i y_i)(\Sigma_{i=1}^n x_i^3)}{(\Sigma_{i=1}^n x_i^2)(\Sigma_{i=1}^n x_i^4) - (\Sigma_{i=1}^n x_i^3)(\Sigma_{i=1}^n x_i^3)} \tag{34}$$

The x_i's and y_i's represent the various fluid flow velocities and normalized pressure drop points respectively taken in the experimental runs. The inertia coefficient and permeability can then be calculated by back solving Eqs. (30) and (31) after knowing (A) and (B).

3.3. Effective thermal conductivity (k_{eff})

In general, the overall thermal conductivity of a porous medium depends in a complex fashion on the geometry of the medium. If the heat conduction in the solid and fluid phases occurs in parallel, then the overall conductivity k_A is the weighted

arithmetic mean of the conductivities of the solid k_s and fluid k_f phases [9]:

$$k_A = (1-\varepsilon)k_s + \varepsilon k_f \tag{35}$$

Calmidi and Mahajan [34] reported experimentally and analytically their **metal foams'** effective thermal conductivity measurements. Experimental work was performed singly with water and with air as fluids. An empirical relationship that correlates the experimental data with an accuracy of 97.5% was developed.

$$k_{eff} = \varepsilon k_f + A(1-\varepsilon)^n k_s \tag{36}$$

The better fit was obtained for $n=0.763$. However, $(A)=0.195$ for water and 0.181 for air. The analytical model was developed based on the structure of the metal foam matrix. The structure was represented by a two-dimensional hexagonal array where the fibers were the edges of the hexagons as shown in Fig. 7.

They supposed that the heat conduction occurs in one dimension to derive an analytical expression for the effective thermal conductivity. Fig. 8 shows the orientation of heat flow:

$$k_{eff} = \left[\left(\frac{2}{\sqrt{3}}\right)\left(\frac{r(b/L)}{k_f+(1+(b/L))((k_s-k_f)/3)}+\frac{(1-r)(b/L)}{k_f+(2/3)(b/L)(k_s-k_f)} + \frac{(\sqrt{3}/2)-(b/L)}{k_f+(4r/3\sqrt{3})(b/L)(k_s-k_f)}\right)\right]^{-1} \tag{37}$$

$$\frac{b}{L} = \frac{-r+\sqrt{r^2+(2/\sqrt{3})(1-\varepsilon)(2-r(1+(4/\sqrt{3})))}}{2/3(2-r(1+(4/\sqrt{3})))}$$

Boomsma and Poulikakos [13] calculated the thermal conductivity by using Fourier's law through the representative section, based on heat conduction through a series of four levels (L_A, L_B, L_C, L_D) which are shown in Fig. 4c, to give the following relation:

$$k_{eff} = \frac{L_A+L_B+L_C+L_D}{(L_A/k_A)+(L_B/k_B)+(L_C/k_C)+(L_D/k_D)} \tag{38}$$

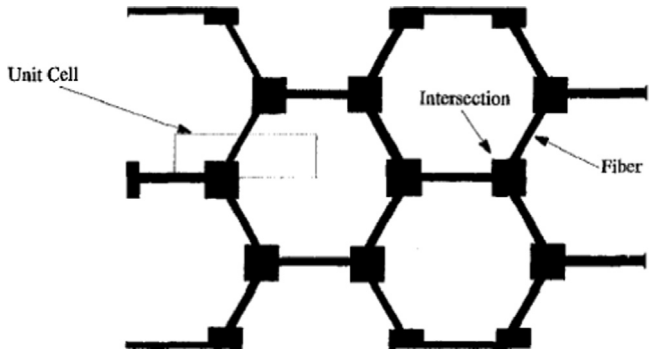

Fig. 7. Hexagonal structure of metal foam matrix, Calmidi and Mahajan [34].

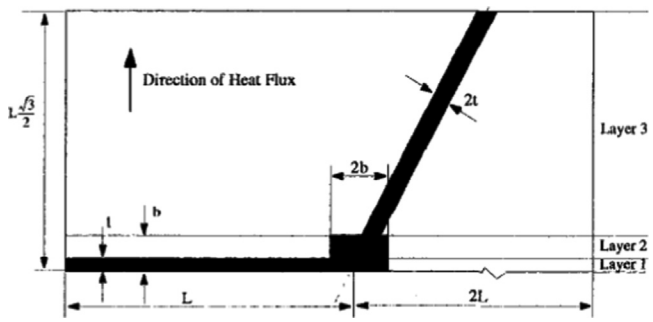

Fig. 8. Unit-cell representation of hexagonal structure, Calmidi and Mahajan [34].

where L_A, L_B, L_C, L_D are the ligament lengths (m) for unit cell subsections A, B, C, and D respectively.

Bhattacharya et al. [16] modified the Calmidi and Mahajan [34] analysis. They replaced the square intersection (Fig. 8) by a circular one as shown in Fig. 9. The effective thermal conductivity was obtained from the model equation as follows:

$$k_{eff} = \left[\left(\frac{2}{\sqrt{3}}\right)\left(\frac{t/L}{k_f+((k_s-k_f)/3)}+\frac{\sqrt{3}/2-(t/L)}{k_f}\right)\right]^{-1} \tag{39}$$

$$\frac{t}{L} = \frac{-\sqrt{3}-\sqrt{3+(1-\varepsilon)(\sqrt{3}-5)}}{1+(1/\sqrt{3})-(8/3)} \tag{40}$$

Phanikumar and Mahajan [35] studied numerically and experimentally the non-Darcy free convection heat transfer in **metal foams**. The fluid and solid effective thermal conductivities (k_f and k_s) were estimated using the empirical relations proposed by Calmidi and Mahajan [34]. They used the following effective thermal conductivity correlation which was proposed by Bhattacharya et al. [16]:

$$k_{eff} = \frac{[M(\varepsilon k_f+(1-\varepsilon)k_s)+(1-M)]}{(\varepsilon/k_f+((1-\varepsilon)/k_s))} \tag{41}$$

Hadim and North [36] studied numerically the forced convection in a **sintered porous channel** with inlet and outlet slots and proposed the thermal dispersion conductivity in the porous matrix which is accounted for as a diffusive term and is added to the stagnant thermal conductivity to get the effective thermal conductivity [37,38].

$$k_{eff} = \textit{Stagnant Thermal Conductivity} + \textit{Thermal Dispersion Conductivity} \tag{42}$$

Hadim and North [36] developed the empirical correlations proposed by Wakao and Kaguei [39] to be suitable for the thermal dispersion conductivity and the sintered porous media stagnant thermal conductivity. In this model, in both directions, the effective thermal conductivities were calculated as

$$(k_{eff})_x = \varepsilon k_f + (1-\varepsilon)k_s + 0.5 PrRe_d\left(\frac{u}{u_m}\right)k_f \tag{43}$$

$$(k_{eff})_y = \varepsilon k_f + (1-\varepsilon)k_s + 0.1 PrRe_d\left(\frac{u}{u_m}\right)k_f \tag{44}$$

Jiang and Lu [27] studied numerically the fluid flow and convective heat transfer of water in **sintered bronze porous plate channels**, and they made comparison for the effective thermal conductivity values between the values which were calculated from the equation proposed by Zehener [40] and their numerical

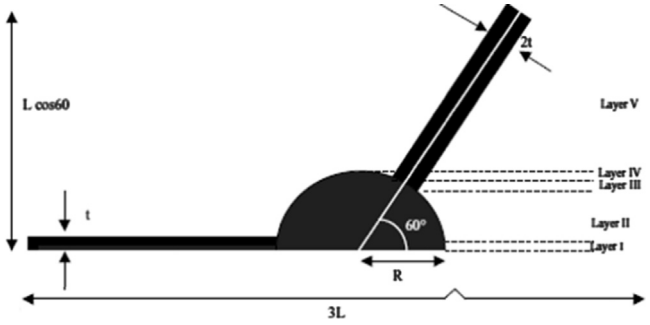

Fig. 9. Unit cell for the circular intersection, Bhattacharya et al. [16].

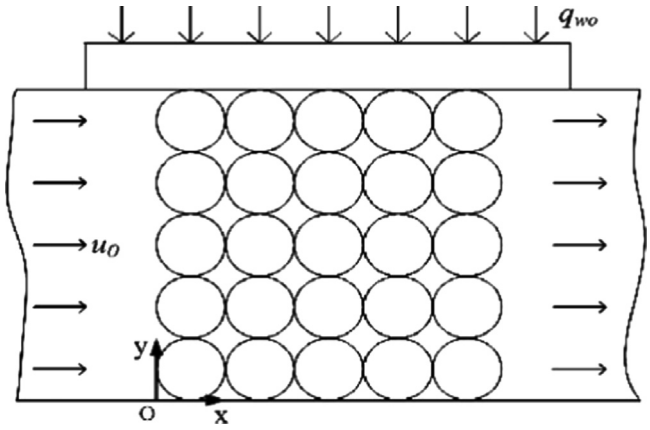

Fig. 10. Schematic diagram of the physical system of Jiang and Lu [27].

results are shown in Fig. 10.

$$k_{eff} = k_f\left((1-\sqrt{1-\varepsilon})+\frac{2\sqrt{1-\varepsilon}}{1-\sigma B}\left[\frac{(1-\sigma)B}{(1-\sigma B)^2}\ln\left(\frac{1}{\sigma B}\right)-\frac{B+1}{2}-\frac{B-1}{1-\sigma B}\right]\right) \tag{45}$$

$$B = 1.25[(1-\varepsilon)/\varepsilon]^{10/9} \tag{46}$$

$$\sigma = \frac{k_f}{k_s} \tag{47}$$

The effective thermal conductivity of the porous media (Fig. 10) from the numerical results was calculated based on Fourier's law using the known heat flux on the top surface and the thickness of the porous media, with the numerically calculated temperature difference between the top and the bottom surfaces. They found in the same porosity of $\varepsilon=0.354$ that the effective thermal conductivity predicted by Eq. (35) was $k_{eff}=0.699$ W/mK, and with numerical calculations was 0.668 W/mk, which differs by 4.4%.

The mechanism of heat transfer due to the fluid motion is known as the convection heat transfer. The convection heat transfer types are dependent on the fluid motion. If the motion of fluid is due to the gradient of existing temperature between the fluid and the solid, the convection heat transfer is known as free (natural) convection. The convection heat transfer is known as forced convection if the motion of fluid is due to external effects. The convection heat transfer is known as mixed convection if the motion of fluid is due to free (natural) and forced convection effects together [41]. Nanofluids that contain mixtures of base fluid with a very small amount of nanoparticles have very high thermal conductivities compared with conventional heat transfer fluids [3]. Porous material with nanofluid exhibit raised convection heat transfer coefficients and effective thermal conductivity compared with conventional heat transfer fluids only. Nanofluids contain base fluids such as ethylene glycol (EG), engine oil (EO), water, acetone, etc. [42], and nanoparticle materials such as dioxide ceramics, aluminum dioxide (Al_2O_3), copper dioxide (CuO), etc. [43].

4. Nanofluid thermophysical properties

In this section, the density, specific heat capacity, effective thermal conductivity and effective viscosity for nanofluid are discussed.

Over the past few years in literature, base nanofluid thermophysical properties have been published. Some data have been provided on temperature-dependent properties, even though they are only for effective thermal conductivity and dynamic viscosity of the nanofluid.

To understand the nanofluid thermophysical properties, studies and formulas should be defined and some variables such as nanoparticle volume fraction and Brownian motion in nanofluid should also be discussed. One important variable in nanofluid studies is nanofluid volume fraction (φ). It is defined as the constituent volume divided by all constituent volumes of the mixture prior to mixing [44], and nanofluid effective thermal conductivity increases with increase in nanoparticles volume fraction [45].

$$\varphi = \frac{V_p}{V_{total}} \tag{48}$$

Brownian motion in nanofluid is defined as the particles random movement. Brownian motion is one of the key heat transfer mechanisms in nanofluids [46,47]. Thermophoresis in nanofluid is defined as migration of the molecules from warmer to cooler areas [48].

4.1. Density

Vajjha et al. [49] measured the nanofluid density by using the density meter for liquids and gases. They found a good agreement between their results and the theoretical equation which was estimated based on the physical principle of the mixture rule and was used by the Pak and Cho [50] equation.

$$\rho_{nf} = \left[\frac{m}{V}\right]_{nf} = \frac{m_p+m_{bf}}{V_p+V_{bf}} = \frac{\rho_p V_p+\rho_{bf}V_{bf}}{V_p+V_{bf}} = \varphi\rho_p+(1-\varphi)\rho_{bf} \tag{49}$$

4.2. Specific heat capacity

The calculation of the effective specific heat of a nanofluid is straightforward. This can be estimated based on the physical principle of the mixture rule. Corcione [51] and Abu-Nada et al. [52] proposed that, the nanofluid specific heat can be calculated by using the following equation which was used by Xuan and Roetzel [53]:

$$\begin{aligned}(\rho c_p)_{nf} &= \rho_{nf}\left(\frac{Q}{m\Delta T}\right)_{nf}\\ &= \rho_{nf}\frac{Q_{bf}+Q_p}{(m_{bf}+m_p)\Delta T}\\ &= \rho_{nf}\frac{(mC_p)_{bf}\Delta T+(mC_p)_p\Delta T}{(m_{bf}+m_p)\Delta T}\\ &= \rho_{nf}\frac{(\rho C_p)_{bf}V_{bf}+(\rho C_p)_pV_p}{(\rho_{bf}V_{bf}+\rho_pV_p)}\\ &= \varphi(\rho c_p)_p+(1-\varphi)(\rho c_p)_{bf}\end{aligned} \tag{50}$$

which can be rewritten as follows:

$$c_{p_{nf}} = \frac{(1-\varphi)(\rho c_p)_{bf}+\varphi(\rho c_p)_p}{(1-\varphi)\rho_{bf}+\varphi\rho_p} \tag{51}$$

4.3. Effective thermal conductivity

Studies regarding the thermal conductivity of nanofluids showed that high enhancements of thermal conductivity can be achieved by using nanofluids. It is possible to obtain thermal conductivity enhancements larger than 20% for a particle volume fraction smaller than 5% [54,55]

From the many experimental results, it is known that the nanofluids effective thermal conductivity and dynamic viscosity depend on many factors such as the nanoparticles thermal conductivities and dynamic viscosity, base fluid thermophysical properties: nanoparticles shape, volume fraction and the operation temperature. Most of the researchers report that increasing the

Table 1
Summary of models for the effective thermal conductivity of nanofluids.

Mechanisms of thermal conductivity enhancement	Studies	Thermal conductivity ratio (k_{nf}/k_{bf})
Brownian motion of nanoparticles	Koo and Kleinstreuer [61]	$\frac{k_p+2k_{bf}+2(k_p-k_{bf})\varphi}{k_p+2k_{bf}-(k_p-k_{bf})\varphi}+\left(5\times10^4\beta\varphi\rho_{bf}(c_p)_{bf}\sqrt{\frac{k_{bf}T}{d_p\rho_p}}f(T,\varphi)/k_{bf}\right)$
	Chon et al. [54]	$1+64.7\varphi^{0.746}\left(\frac{d_{bf}}{d_p}\right)^{0.369}\left(\frac{k_p}{k_{bf}}\right)^{0.7476}Pr^{0.9955}Re^{1.2321}$
	Xu et al. [62]	$\frac{k_p+(n-1)k_{bf}-2(n-1)(k_p-k_{bf})\varphi}{k_p+(n-1)k_{bf}+(k_{bf}-k_p)\varphi}k_{bf}+C\,k_{bf}\frac{Nu.d_{bf}(2-D_{bf})D_{bf}[(d_{p.\,max}./d_{p.\,max}.)^{1-D_{bf}}-1]^2}{Pr(1-D_{bf})^2\,(d_{p.\,max}./d_{p.\,max}.)^{2-D_{bf}}-1}\times\frac{1}{d_p}$
Clustering of nanoparticles	Xuan et al. [63]	$\frac{k_p+2k_{bf}-2\varphi(k_{bf}-k_p)}{k_p+2k_{bf}+\varphi(k_{bf}-k_p)}+\frac{\rho_p\varphi c_{p_p}}{2k_{bf}}\sqrt{\frac{k_pT}{3\pi r_{cl}\mu_{bf}}}$
	Prasher et al. [64]	$\frac{k_{cl}+2k_{bf}+2\varphi(k_{cl}-k_{bf})}{k_{cl}+2k_{bf}-\varphi(k_{cl}-k_{bf})}$
Liquid layering around nanoparticles	Yu and Choi [65]	$\frac{k_{pe}+2k_{bf}+2\varphi(k_{pe}-k_{bf})(1-\beta)^3}{k_{pe}+2k_{bf}-\varphi(k_{pe}-k_{bf})(1+\beta)^3}$ $k_{pe}=\frac{2(1-\gamma)+(1+\beta)^3(1+2\gamma)}{-(1-\gamma)(1+\beta)^3(1+2\gamma)}k_p$ $\gamma=\frac{k_{layer}}{k_p},\beta=\frac{nano-layer\ thickness}{original\ particle\ radius}$

thermal conductivity increases the particle volume fraction and the relation found is usually linear [56,57].

Presently, there are no theoretical formulas available to predict the thermal conductivity of nanofluids satisfactorily. However, there exist several semi-empirical correlations for calculating the apparent conductivity of two-phase mixtures. They are mainly based on the following definition of the effective thermal conductivity of a two-component mixture [58]:

$$k_{eff}=\frac{k_p\varphi_p(dT/dx)_p+k_{bf}\varphi_{bf}(dT/dx)_{bf}}{\varphi_p(dT/dx)_p+\varphi_{bf}(dT/dx)_{bf}} \tag{52}$$

More than a century ago, Maxwell derived an equation for calculating the effective thermal conductivity of solid–liquid mixtures consisting of spherical particles [59]:

$$k_{eff}=\frac{(k_p+2k_{bf})+2(k_p-k_{bf})\varphi}{(k_p+2k_{bf})-(k_p-k_{bf})\varphi} \tag{53}$$

Maxwell's formula shows that the effective thermal conductivity of nanofluids relies on the thermal conductivity of the spherical particle, the base fluid and the volume fraction of the solid particles. In Özerinç et al. [57], and Wang and Mujumdar [58] reviews, many theoretical studies were done and several mechanisms were proposed in order to explain the thermal conductivity enhancement obtained with nanofluids. In this section, summary of some developed models for the prediction of the effective thermal conductivity of nanofluids based on mechanisms of thermal conductivity enhancement in nanofluids is provided in Table 1.

4.4. Effective viscosity

Einstein [60], was the first to calculate the effective viscosity of a suspension of spherical solids. By assuming that the disturbance of the flow pattern of the matrix base fluid caused by a given particle does not overlap with the disturbance of flow caused by the presence of a second suspended particle, he derived the following equation:

$$\frac{\mu_{nf}}{\mu_{bf}}=1+2.5\varphi \tag{54}$$

Some recent theoretical formulations developed especially for nanofluids were listed by Wang and Mujumdar [58]. Some of these equations are provided in Table 2.

Table 2
Different effective dynamic viscosity formulas for nanofluid.

Studies	Viscosity ratio (μ_{nf}/μ_{bf})
Maïga et al. [66]	$1+7.3\varphi+123\varphi^2$
Koo and Kleinstreuer [67]	$\frac{1}{(1-\varphi)^{2.5}}+\frac{1}{\mu_{bf}}\times5\times10^4\beta\varphi\rho_{bf}\sqrt{\frac{k_{bf}T}{D_p\rho_p}}f(T,\varphi)$
He et al. [68]	$199.21\varphi^2+4.62\varphi+1$
Corcione [51]	$\frac{1}{1-34.87(d_p/d_{bf})^{-0.3}\varphi^{1.03}},\quad d_{bf}=\left(\frac{6M}{N\pi\rho_{bf_o}}\right)^{1/3}$

5. Studies on convection heat transfer and fluid flow in porous media with nanofluid

Convection heat transfer in porous media has been studied extensively for over 150 years now [16]. The deference of the effective factors on the heat transfer and fluid flow through porous media with nanofluid led to diversity of studies in this field, these factors are

- Boundary conditions in porous media, which include either the porous media is penetrative as an open cell aluminum foam or non-penetrative as a closed cell aluminum foam.
- Thermal conditions in convection heat transfer, which include either convection heat transfer with constant temperature or with constant heat flux, or both.
- Porous media shapes are either rectangular or triangular etc.
- Working fluid types are either nanofluid (Al_2O_3+water), (SiO_2+water) or conventional fluid (air, water, oil, etc.).
- The method of data processing includes numerical, analytical, or experimental.
- Convection heat transfer types include free (natural), forced or mixed convection.

Many studies have been done on heat transfer in porous media with nanofluid to predict the effects of porous media and nanofluid characteristics on natural, forced and mixed convection heat transfer as shown below.

5.1. Natural convection

Nield and Kuznetsov [69] studied analytically the onset of free convection heat transfer in a horizontal layer of a porous media filled with a nanofluid. The effects of thermophoresis and Brownian motion on heat transfer were investigated. The results showed that the critical thermal Rayleigh number could be reduced or increased by a substantial amount, depending on whether the basic nanoparticle distribution was top-heavy or bottom-heavy, in the presence of the nanoparticles. Oscillatory instability was possible in the case of a bottom-heavy nanoparticle distribution.

Kuznetsov and Nield [70] studied analytically the free convective boundary-layer flow of a nanofluid past a vertical plate. The effects of thermophoresis and Brownian motion on the Nusselt number were investigated. Their findings indicated that the Nusselt number increased when buoyancy-ratio, Brownian motion and thermophoresis parameters increased.

Sun and Pop [71] studied numerically the steady-state natural convection heat transfer behavior of nanofluid inside a right-angle triangular enclosure saturated by a porous media as shown in Fig. 11. The effects of Cu, TiO_2 and Al_2O_3 with water as base fluid, Rayleigh number, size of heater, position of heater, volume fraction and enclosure aspect ratio on the average Nusselt number were investigated. Their findings indicated that the maximum value of average Nusselt number was obtained with the highest value of Rayleigh number, by lowering the heater position and decreasing the enclosure aspect ratio and the largest heater size. When using Cu nanoparticle, the highest average Nusselt number value was obtained.

Chamkha et al. [72] studied numerically the non-similar solution for free convective heat transfer boundary layer flow over isothermal sphere embedded in porous media filled with a nanofluid as shown in Fig. 12. The influences of Brownian motion, buoyancy ratio parameter, Lewis number and thermophoresis on the surface heat and mass transfer rates and friction factor were investigated. Their findings indicated that the friction factor increased when thermophoresis and buoyancy ratio increased, whereas the heat and mass transfer rates decreased. The mass transfer rates and friction factor increased when Brownian motion increased, whereas the heat transfer rate decreased.

Rashad et al. [73] studied numerically the natural convection boundary layer of a non-Newtonian fluid over a permeable vertical cone embedded in a porous media filled with a nanofluid as shown in Fig. 13. The effects of the Brownian motion parameter, buoyancy ratio, Lewis number and thermophoresis parameter on the Nusselt and Sherwood numbers were investigated. Their findings indicated that the Nusselt and Sherwood numbers decreased when buoyancy ratio increased. The Nusselt number decreased while the Sherwood number increased when the Brownian motion parameter increased.

Hady et al. [74] studied numerically the influence of heat generation absorption on free convective boundary layer flow from a vertical cone embedded in a porous media saturated by nanofluid as shown in Fig. 14. The influence of the heat generation absorption parameter on the Nusselt number was investigated. Their findings indicated that as the heat generation absorption parameter increased, the local Nusselt number decreased.

Nield and Kuznetsov [75] studied analytically Cheng and Minkowycz's [76] problem for the double-diffusive free convection heat transfer past a vertical plate boundary layer flow in a porous media filled with a nanofluid. The effects of thermophoresis parameter and Brownian motion parameter on heat transfer were investigated. Their findings indicated that Nusselt number increased when the thermal boundary layer thickness, thermophoresis and Brownian motion parameters increased and regular buoyancy ratio decreased.

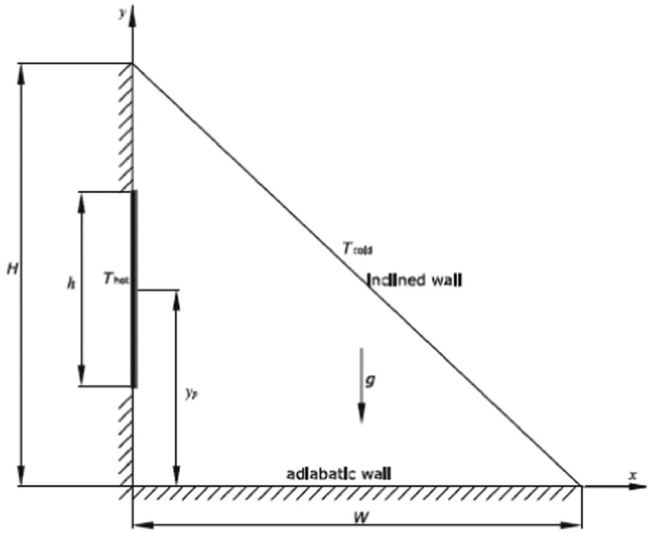

Fig. 11. Sketch of the physical model of Sun and Pop [71].

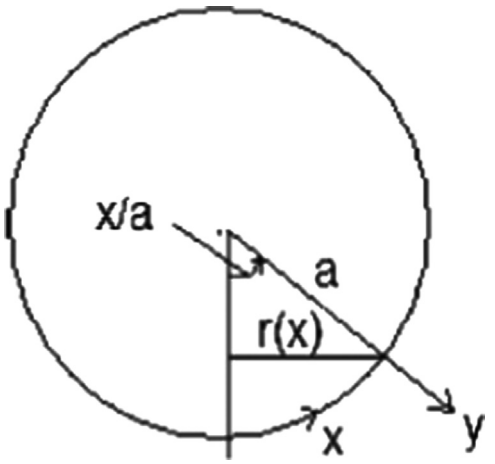

Fig. 12. Schematic diagram of the physical model of Chamkha et al. [72].

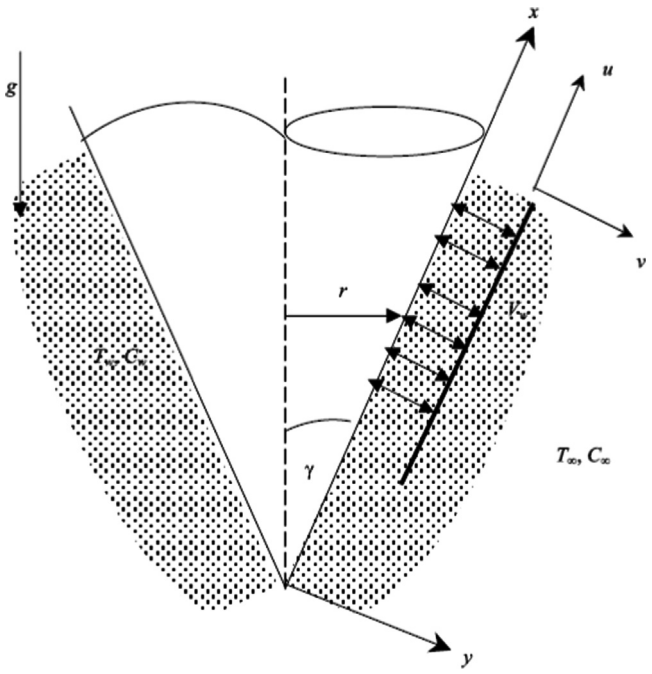

Fig. 13. Flow model and physical coordinate system of Rashad et al. [73].

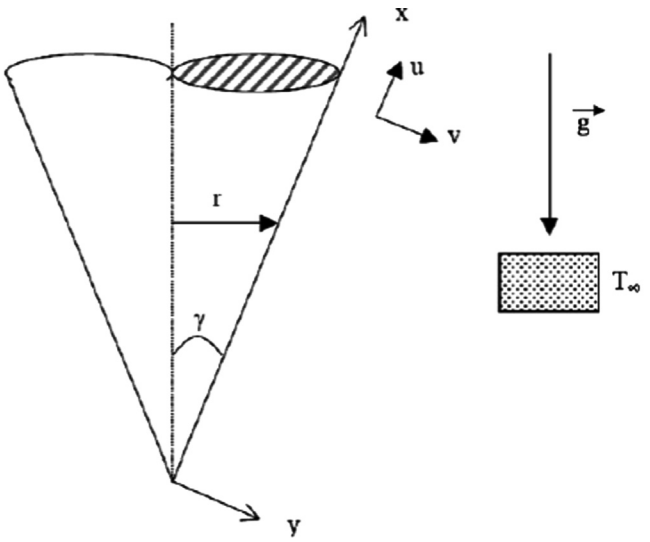

Fig. 14. Flow model and physical coordinate system of Hady et al. [74].

Kuznetsov and Nield [77] studied analytically the free convective boundary-layer flow of a nanofluid past a vertical plate with constant nanoparticle volume fraction and temperature. The effects of the Prandtl number, nanofluid Lewis and regular Lewis numbers, nanofluid buoyancy-ratio parameter, Brownian motion and thermophoresis parameters on the heat transfer were investigated. Their findings indicated that the reduced Nusselt number was a decreasing function of each thermophoresis parameter, and Brownian motion parameter. Variation of the regular buoyancy ratio produced a change in regular Nusselt number in either direction.

Bhadauria et al. [78] studied numerically the linear and nonlinear thermal instabilities in a horizontal porous media filled with a nanofluid cooled from above and heated from below. The results revealed that convection heat transfer was obtained through oscillatory mode when horizontal wave number was small. The convection heat transfer mode for onset of thermal instability became stationary on increasing horizontal wave number. Also that nonlinear finite amplitude was the preferred convection heat transfer mode earlier to oscillatory mode.

Hady et al. [79] studied numerically the effect of yield stress on natural convective boundary-layer flow of a non-Newtonian nanofluid past a vertical plate in a porous media. The influences of power law index, yield stress parameter, Lewis and Brownian motion numbers, buoyancy ratio and a thermophoresis number were investigated. The results indicated that the Nusselt and Sherwood numbers increased when the velocity distribution, Lewis number and power index of non-Newtonian fluid increased. The Nusselt and Sherwood numbers decreased when thermophoresis and buoyancy ratio increased.

Khan and Aziz [80] studied numerically the double-diffusive free convection from a vertical plate to a porous media saturated with a binary base fluid containing nanoparticles. This work extended the work of Nield and Kuznetsov [75] where the nanoparticles fluxes specified and vertical surface had heat solute as a power law function of the distance along the surface as shown in Fig. 15. The influences of the exponent of the power law on the heat and mass transfer characteristics were investigated. The results showed that the reduced nanoparticle Sherwood number was significantly higher for double diffusion in regular and nanofluids than it was for mono-diffusion in regular and nanofluids; and in both cases it increases as the exponent dimensionless solutal concentration increased, and the reduced nanoparticle Sherwood number largely depended on the diffusion process (mono or double) and little was affected by the fluid (regular or nano).

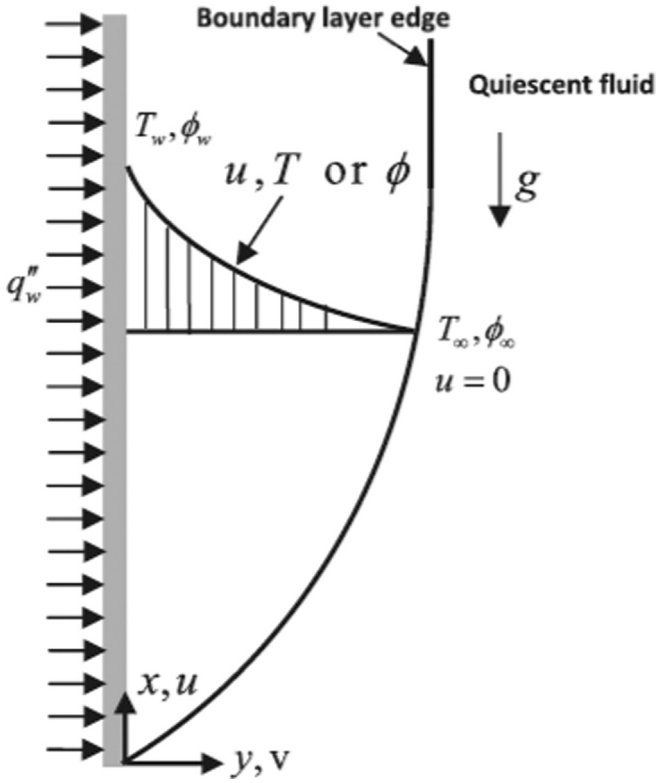

Fig. 15. Vertical surface in a porous medium saturated with a fluid containing solute and with nanoparticles in suspension, Khan and Aziz [80].

Aziz et al. [81] studied numerically the steady boundary layer free convection heat transfer and fluid flow past a horizontal flat plate embedded in a porous media saturated with a nanofluid containing gyrotactic microorganisms. The effects of bio-convection parameters on the dimensionless temperature, velocity, density and nanoparticle concentration of the Sherwood, local Nusselt and motile microorganism numbers were investigated. The results showed that no appreciable effect of the bio-convection parameters on nanoparticle concentration and temperature distributions in the flow field was observed. The buoyancy parameter has a significant impact on density and velocity of motile microorganisms profiles. The Sherwood and local Nusselt number of the motile microorganisms increased as bio-convection Rayleigh, Lewis and Péclet numbers increased but they decreased with the increase in buoyancy ratio parameter.

Agarwal et al. [82] studied the double-diffusive convection heat transfer in a horizontal porous media filled with a nanofluid, cooled from above and heated from below, for the case when the base fluid of the nanofluid was itself a binary fluid such as salty water. The effects of the thermo-solutal Lewis and thermo-nanofluid Lewis numbers, dufour parameter, soret parameter, porosity, solutal Rayleigh number and modified diffusivity ratio on the stabilized system were investigated. The results showed that the thermo-solutal Lewis and thermo-nanofluid Lewis numbers, dufour parameter, soret parameter and porosity tended to stabilize the system, while solutal Rayleigh number and modified diffusivity ratio tended to destabilize the system.

Cheng [83] studied numerically the free convection boundary layer flow over a truncated cone in a porous media filled with a nanofluid with constant temperature and nanoparticle volume fraction as shown in Fig. 16. The influences of the thermophoresis and Brownian motion parameters, buoyancy ratio and Lewis number on the Nusselt number and velocity and temperature profiles were investigated. Their findings indicated that the local

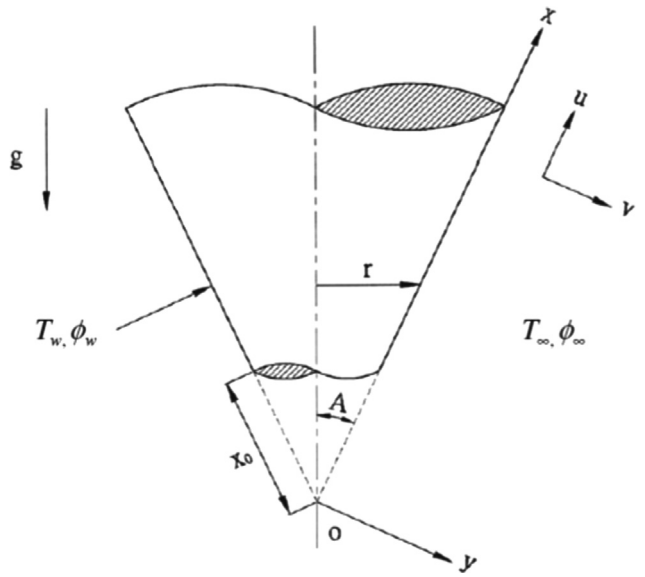

Fig. 16. Flow model and physical coordinate system of Cheng [83].

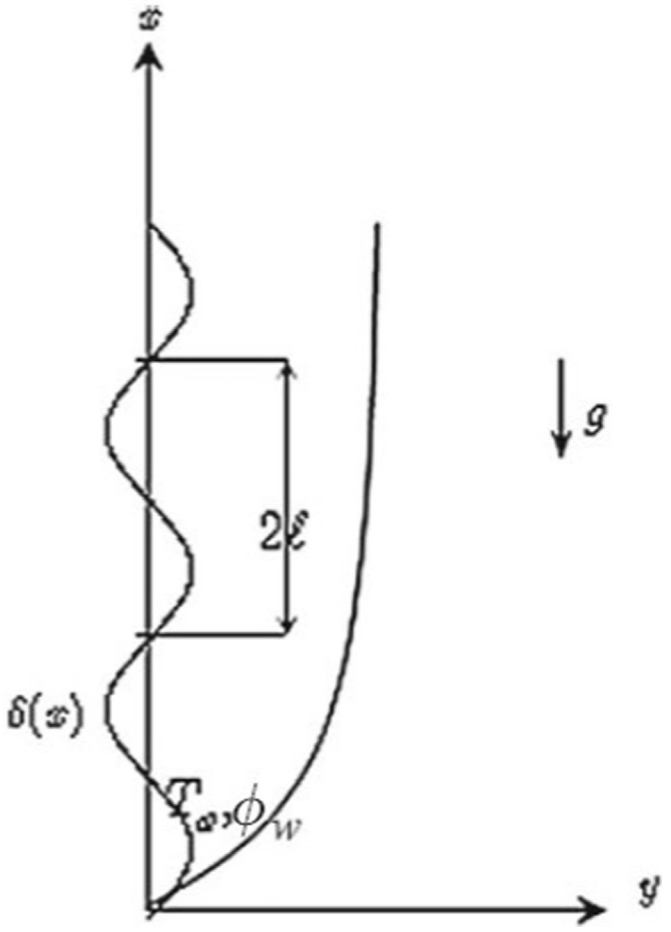

Fig. 17. Flow model and physical coordinate system of Mahdy and Ahmed [84].

Nusselt number decreased when thermophoresis parameter or the Brownian parameter increased. Since, the Lewis number and buoyancy ratio was decreased, the local Nusselt number increased.

Mahdy and Ahmed [84] studied numerically the two-dimensional steady natural convection heat transfer over a vertical wavy surface embedded in a porous media filled with a nanofluid as shown in Fig. 17. The wavy surface profile was given by $y = \delta(x) = a \sin(\pi x/\ell)$, where (a) is the amplitude of the wavy surface and ℓ is the characteristic half length of the wavy surface. The effects of buoyancy ratio number, Brownian motion, wavelength ratio and thermophoresis parameter on heat and mass transfer rates were investigated. Their findings indicated that increasing thermophoresis parameter, buoyancy ratio number, and Brownian motion parameter, decreased the convection heat and mass transfer rates.

Yadav et al. [85] studied numerically the influence of internal heat source on the onset of Darcy–Brinkman convection in a porous layer filled with a nanofluid as shown in Fig. 18. The influences of nanoparticle Rayleigh number, internal heat source strength, modified particle-density increment, Lewis number, porosity and Darcy number on the stability of the system were investigated. Their findings indicated that the nanoparticle Rayleigh number, internal heat source, Lewis number and modified diffusivity ratio had a destabilizing effect, while the porosity and Darcy number showed stabilizing influences on the system.

Cheng [86] studied numerically the steady laminar natural convection boundary layer flow over elliptic cross section horizontal

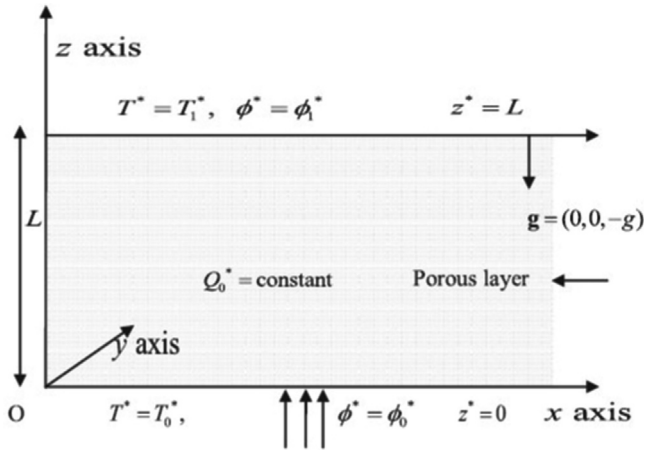

Fig. 18. Sketch of the problem geometry and coordinates of Yadav et al. [85].

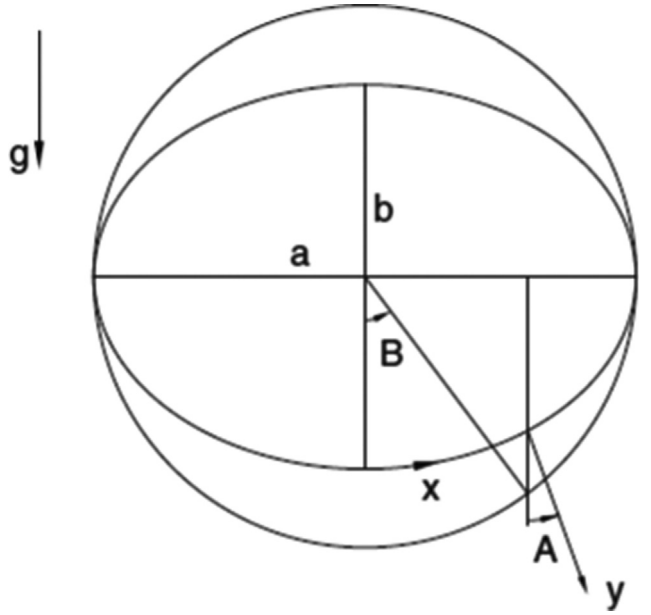

Fig. 19. Coordinate system for an elliptical cylinder of blunt orientation of Cheng [86].

cylinder embedded in porous media saturated by a nanofluid with constant volume fraction and wall temperature as shown in Fig. 19. The influences of thermophoresis and Brownian motion on velocity and temperature profiles were incorporated into the nanofluids model. Their findings indicated that the Nusselt number increased as the Brownian motion or the thermophoresis parameters decreased. As the Lewis number or the buoyancy ratio decreased, the Nusselt number increased.

Chand and Rana [87] studied numerically the influence of rotation on the onset of thermal convection heat transfer in a horizontal layer of nanofluid filled with porous media as shown in Fig. 20. The effects of the Darcy, Lewis, and Rayleigh number as well as modified diffusivity ratio on the stability of the system were investigated. Their findings indicated that the modified diffusivity ratio and Lewis number stabilized the stationary convection. The Darcy number had stabilizing effect on the system in the absence of rotation.

Uddin et al. [88] studied numerically the steady laminar incompressible natural convection heat transfer with nanofluid flow over a permeable upward facing horizontal plate located in porous media taking into account the thermal convective boundary condition as shown in Fig. 21. The effects of nanoparticle volume fraction, Lewis number and Brownian motion on the rate of heat transfer were investigated. Their findings indicated that when the Brownian motion, Lewis number and nanoparticle volume fraction increased the heat transfer rate increased.

Chand and Rana [89] studied analytically the oscillatory convection heat transfer in a horizontal layer of nanofluid in porous media as shown in Fig. 22. The effects of concentration Rayleigh, Lewis and Prandtl–Darcy numbers and modified diffusivity ratio on the oscillatory convection were investigated. Their findings indicated that the Prandtl–Darcy and Lewis numbers and modified diffusivity ratio destabilized the oscillatory convection.

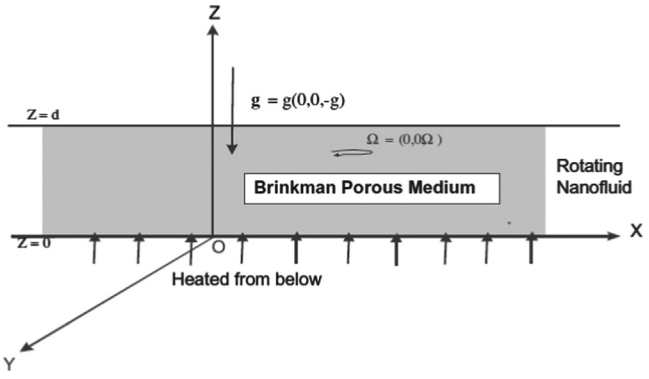

Fig. 20. Schematic sketch of physical situation of Chand and Rana [87].

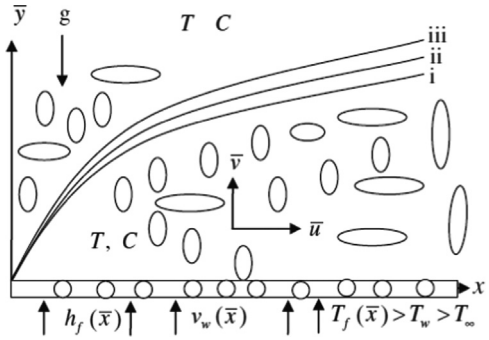

Fig. 21. Coordinate system and flow model of Uddin et al. [88]: (i) nanoparticle volume fraction, (ii) thermal and (iii) momentum boundary layers.

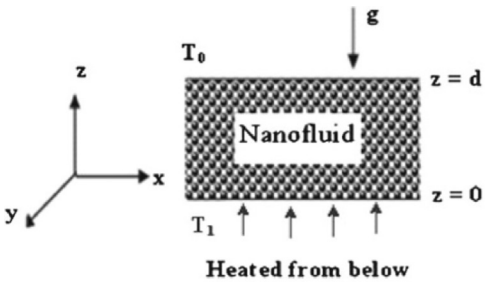

Fig. 22. Physical configuration of Chand and Rana [89].

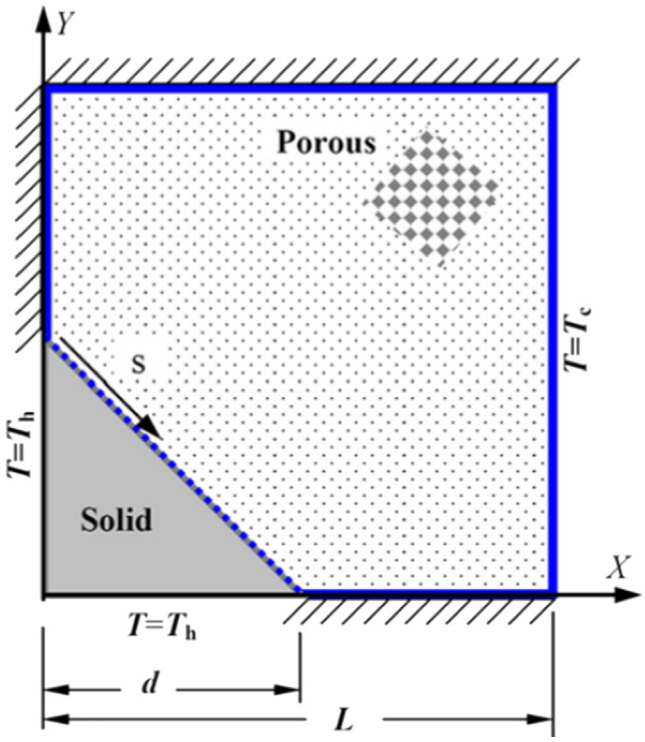

Fig. 23. Physical domain and coordinate system of Chamkha and Ismael [90].

Chamkha and Ismael [90] studied numerically the conjugate free convection–conduction heat transfer in a square domain composed of nanofluids filled porous cavity heated by a triangular solid wall under steady-state conditions as shown in Fig. 23. At the same hot temperature, the horizontal and vertical triangular solid walls were kept isothermal. The other boundaries surrounding the porous cavity were kept adiabatic except the right vertical wall where it was kept isothermally at a lower temperature. The effects of Rayleigh number, nanoparticles volume fraction, solid wall to base-fluid saturated porous media, triangular wall thickness and thermal conductivity ratio on the heat transfer were investigated. Their findings indicated that when the wall thickness was greater than a critical value, the heat transfer enhancement occurred and this critical value became larger when Rayleigh number increased. The copper nanoparticles gave average Nusselt number values greater than the aluminum oxide and titanium dioxide nanoparticles types.

Khan et al. [91] studied numerically the free convection of nanofluids along a vertical plate in porous media. It was assumed that the medium contains gyrotactic microorganisms along with nanoparticles and the plate was subject to prescribed temperature, density of motile microorganisms and concentration of nanoparticles. The effects of bio-convection Rayleigh, Péclet and Lewis numbers were investigated. The results indicated that the

dimensionless temperature, velocity, nanoparticle concentration and the density of motile microorganisms depended strongly on these bio-convection numbers. The dimensionless Sherwood and local Nusselt numbers increased with the decrease in the bio-convection Rayleigh number and increase in bio-convection Péclet and Lewis number.

Umavathi and Mohite [92] studied numerically the linear and nonlinear stability analysis for the onset of convection in a horizontal layer of a porous medium saturated by a nanofluid. The effect of various parameters on the stationary and oscillatory convection was investigated. They also studied the effect of time on transient Nusselt number and Sherwood number which was found to be oscillating when time was small. However, when time becomes very large both the transient Nusselt value and Sherwood value approached their steady state values.

5.2. Forced convection

Ghazvini and Shokouhmand [93] studied analytically and numerically the forced convection heat transfer and nanofluids flow with (0–0.04) volume fraction as coolant through a micro-channel heat sink with constant heat flux as shown in Fig. 24. Two joint analytical approaches were used: the porous media and fin approach. The effects of Brownian–Reynolds number, volume fraction, porosities and channel aspect ratios on heat transfer coefficient and temperature distribution were investigated. Their findings indicated that the porous media approach exhibits a smaller value for both dimensionless temperatures for solid and dimensionless temperature for nanofluid than the fin approach. Both porous media and fin approaches, an increase in channel aspect ratios and bulk temperature, lead to Brownian motion and particle speed increase and due to that, the best heat transport would be possible; so in both approaches an increase in porosity leads to an increase in dimensionless temperature.

Chena and Ding [48] studied numerically the forced convection heat transfer and fluid flow in microchannels heat sink with different concentrations of nanofluids (γAl_2O_3–water) as shown in Fig. 25. The effects of the inertial force term on the micro-channel heat sink performance and the heat transfer characteristics were investigated. Their findings indicated that the inertial force did not affect the temperature distribution of the channel wall, while the total thermal resistance and the fluid temperature distribution changed significantly due to the inertial force effect.

Bachok et al. [94] studied numerically the steady forced convection heat transfer and fluid flow over a rotating porous disk with a constant angular velocity in a nanofluid as shown in Fig. 26, using three nanoparticles types: alumina oxide, copper oxide and titanium dioxide. The surface of the rotating disk was kept at a uniform temperature. The effective thermal conductivity of the nanofluid was presented in two models, namely the Patel and Maxwell–Garnett models. The effects of the suction–injection parameter and nanoparticle volume fraction parameter on the heat transfer and fluid flow were investigated. Their findings indicated that the heat transfer rate and Patel model at the surface increased for both suction and injection, whereas different behaviors were observed for the Maxwell–Garnett model.

Das [95] studied numerically the convective heat transfer and slip flow of nanofluids over a permeable stretching surface as shown in Fig. 27. Two nanoparticles types namely Al_2O_3 and Cu were considered by using water as base fluid with nanoparticle volume fraction (0–0.02). The effects of suction–injection parameter and slip parameter on heat transfer were investigated. His findings indicated that an increase in the nanoparticle volume fraction and slip and injection velocities led to increase in the thermal boundary layer thickness but an opposite effect occurred for suction velocity.

Maghrebi et al. [96] studied numerically the porous channel forced convection heat transfer of nanofluids as shown in Fig. 28.

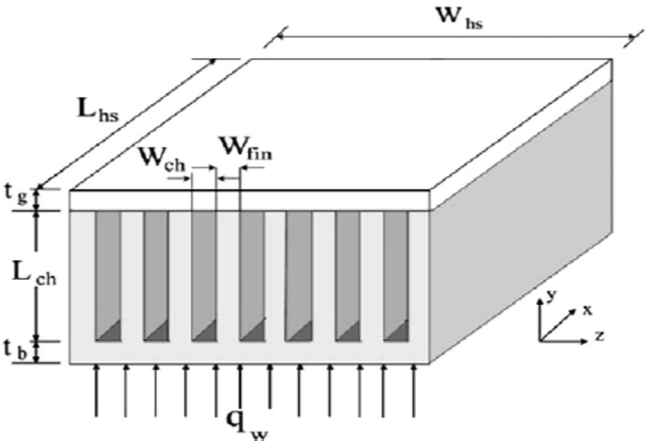

Fig. 24. Schematic diagram of Ghazvini and Shokouhmand [92].

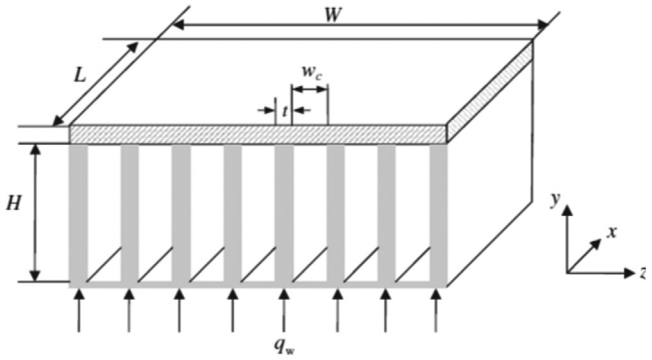

Fig. 25. Schematic diagram of the physical model of Chen and Ding [48].

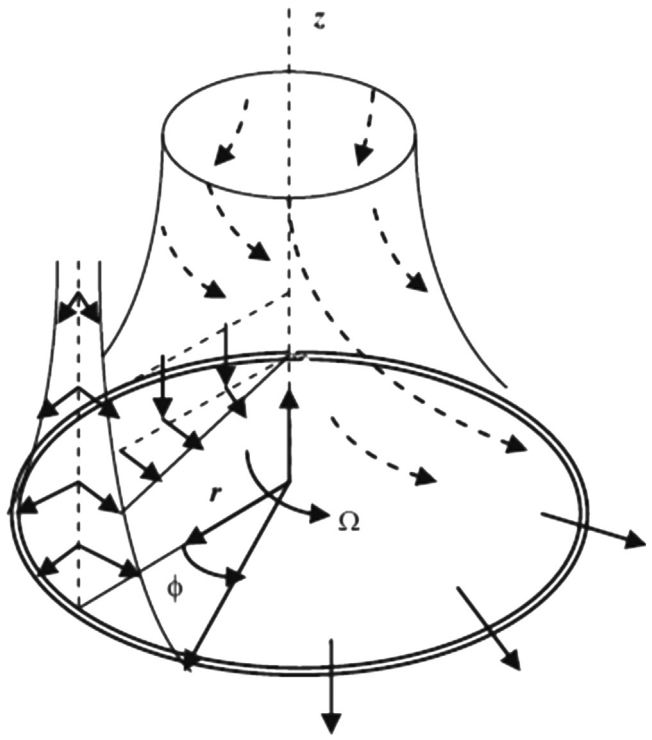

Fig. 26. Physical model and coordinate system of Bachok et al. [93].

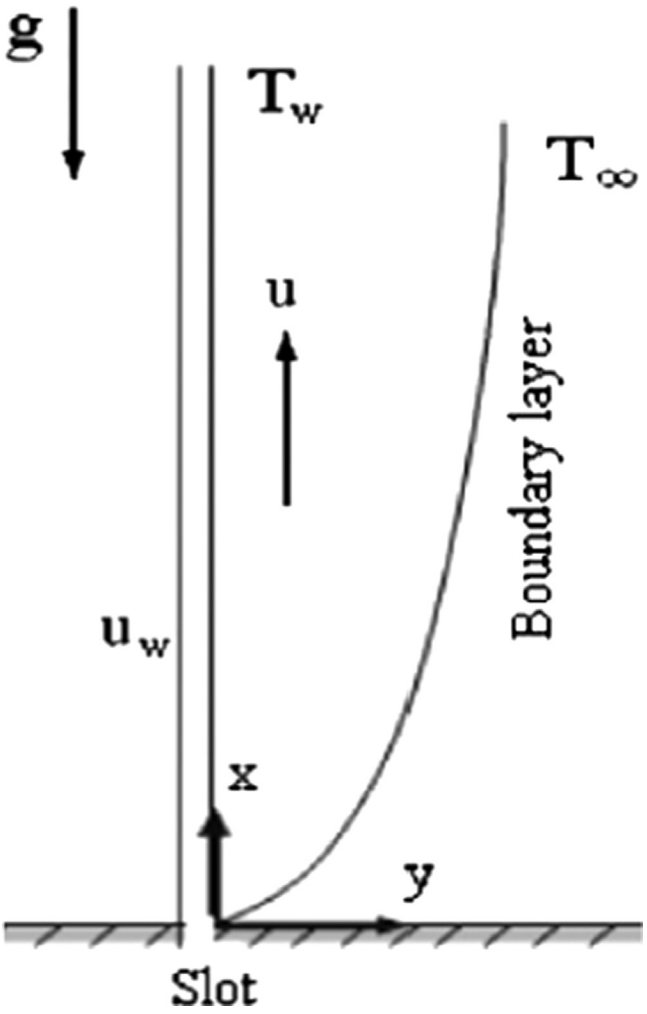

Fig. 27. Physical model and coordinate system of the problem of Das [94].

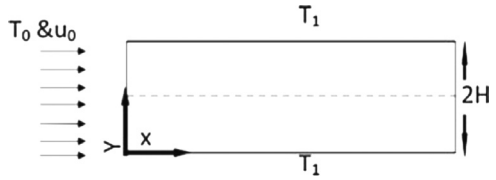

Fig. 28. Geometry of problem and system of coordinate of Maghrebi et al. [95].

The effects of Schmidt and Lewis numbers, thermophoresis and Brownian diffusion on the heat transfer were investigated. Their findings indicated that when the Lewis number increased, the local Nusselt number decreased. The wall temperature gradient and local Nusselt number decreased when the Schmidt number increased.

Servati et al. [97] studied numerically the magnetic field effects on force convection flow of a nanofluid in a channel partially filled with porous media using Lattice Boltzmann method as shown in Fig. 29. The effects of various volume fractions of nanoparticles and different magnitudes of magnetic field on the rate of heat transfer were thoroughly explored. The result shows that the step approximation which is used for the complex boundaries of porous medium is reliable. By raising the nanoparticle volume fraction, average temperature and velocity at the outlet of the channel increase and the average Nusselt number increases dramatically. The increase in the Hartmann number leads to a slow growth of the average Nusselt number, although the outlet average temperature and velocity show a little drop.

Hosseini et al. [98] studied numerically the thermal analysis of rotating system with porous plate using nanofluid. The lower plate is a stretching sheet and the upper one is a solid porous plate as shown in Fig. 30. Copper (Cu) as nanoparticle and water as its base fluid have been considered. The results for the flow and heat transfer characteristics were obtained for various values of the nanoparticle volume fraction, suction–injection parameter, rotation parameter and Reynolds number. The results show that for both suction and injection, the heat transfer rate at the surface has direct relationship with nanoparticle volume fraction, Reynolds number and injection–suction parameter but it has a decreasing function of power for the rotation parameter.

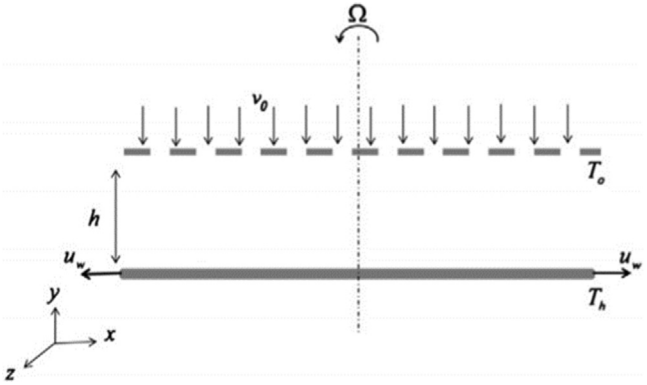

Fig. 30. Schematic diagram of the physical system of Hosseini et al. [98].

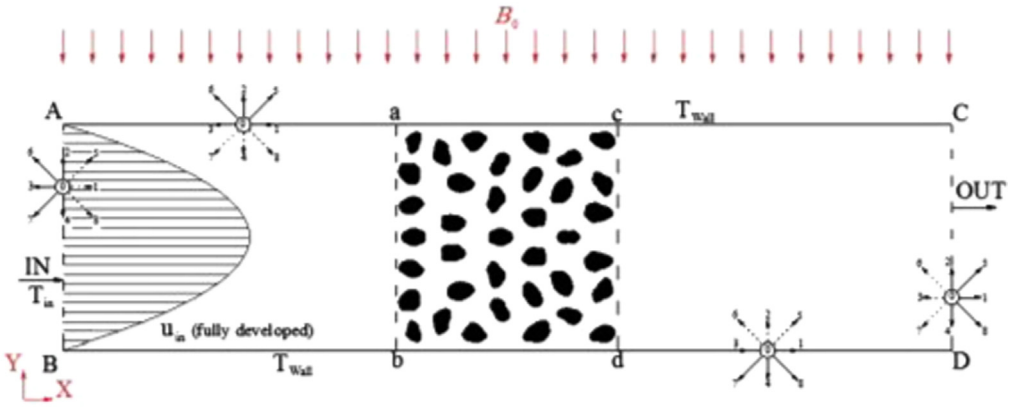

Fig. 29. Geometry of problem and system of coordinate of Javaherdeh and Ashorynejad [97].

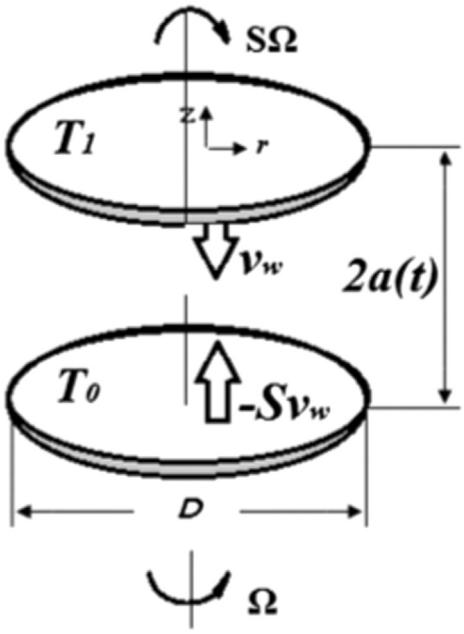

Fig. 31. Sketch of the problem geometry and coordinates of Hatami et al. [99].

Hatami et al. [99] studied numerically the asymmetric laminar flow and heat transfer of nanofluid between contracting rotating disks as shown in Fig. 31. The fluid in the channel was water containing different nanoparticles such as Cu, Ag and Al_2O_3. The effects of the nanoparticle volume fraction, rotational Reynolds number, injection Reynolds number and expansion ratio on flow and heat transfer were considered. The results show that temperature profile becomes more flat near the middle of the two disks with the increase of injection but opposite trend is observed with increase of expansion ratio.

5.3. Mixed convection

Ahmad and Pop [100] studied numerically the steady mixed convection boundary layer flow past a vertical flat plate embedded in a porous media saturated by nanofluids. The basic fluid was water and the different types of nanoparticles were Al_2O_3, Cu and TiO_2. The effects of mixed convection parameters and volume fraction were investigated. The results indicated that the solution had two branches in a certain range of the parameters.

Nazar et al. [101] studied numerically the steady laminar mixed convection boundary layer flow over an isothermal horizontal cylinder embedded in a porous media saturated by a nanofluid for both cases of a cooled and heated cylinder. The effects of mixed convection parameter, nanoparticle volume fraction and nanoparticles types on mixed convection heat transfer and the fluid flow were investigated. Their findings indicated that an increase in the value of the nanoparticle volume fraction led to an increase in the value of mixed convection heat transfer rate and decrease in the magnitude of the skin friction coefficient. The skin friction coefficient values were the highest with nanoparticles Cu compared to the TiO_2 and nanoparticles alumina oxide.

Gorla et al. [102] studied numerically the two-dimensional mixed convective boundary layer flow over a vertical wedge embedded in a porous media filled with a nanofluid as shown in Fig. 32. The effects of the Brownian motion parameter, buoyancy ratio parameter, Lewis number and thermophoresis parameter on the mass transfer rates and friction factor were investigated. Their findings indicated that the friction factor increased when thermophoresis parameter and buoyancy ratio parameter increased,

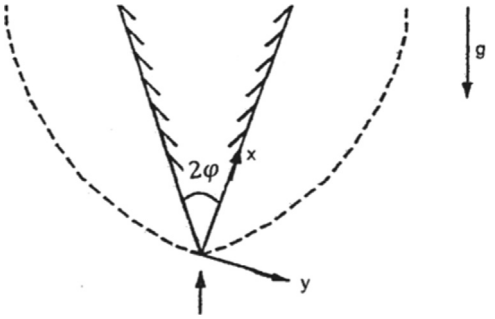

Fig. 32. Flow model and physical coordinate system of Gorla et al. [102].

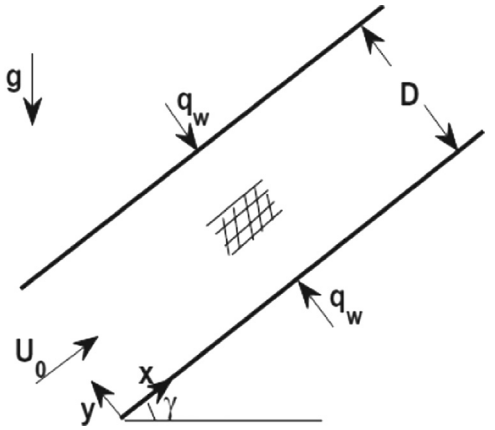

Fig. 33. The channel configuration of Cimpean and Pop [103].

whereas the mass transfer and heat transfer rates decreased. As Brownian motion parameter increased, the mass transfer rates and friction factor increased, whereas the heat transfer rate decreased. As Lewis number increased, the heat transfer rate decreased, whereas the mass transfer rate increased. The heat and mass transfer rates increased when the wedge angle increased.

Cimpean and Pop [103] studied numerically the steady fully developed mixed convection flow of three nanofluids types, copper, alumina oxide and titanium dioxide, with water as their base fluid in an inclined channel saturated by a porous media as shown in Fig. 33. The walls of the channel were heated by a uniform heat flux and a constant flow rate was considered throughout the channel. The effects of the Péclet number, mixed convection parameter, inclination angle of the channel to the horizontal and the volume fraction with three different nanofluids types on the heat transfer were investigated. Their findings indicated that the heat transfer increased with nanofluid, even for small additions of nanoparticles in the base fluid.

Hajipour and Dehkordi [104] studied analytically and numerically the mixed convection heat transfer of nanofluids in a vertical channel partially saturated by highly porous media as shown in Fig. 34. The channel's walls were kept at constant temperatures T_{w1} and T_{w2}, where $T_{w2} > T_{w1}$. The effects of Brownian motion and thermophoresis on the velocity and temperature profiles and Nusselt number values were investigated. Their findings indicated that with increasing nanoparticle mass flux, the Nusselt number at the cold wall (Nu_1) increased. With increasing buoyancy force and viscous dissipation, the nanofluid velocity and temperature increased. The heat transfer rate from the nanofluid to the cold wall ($Nu_1 > 0$) increased with an increase in the buoyancy force and viscous dissipation. Until the heat transfer direction changed and became from the nanofluid to the hot wall, the heat transfer rate from the hot wall to the nanofluid ($Nu_2 > 0$) decreased.

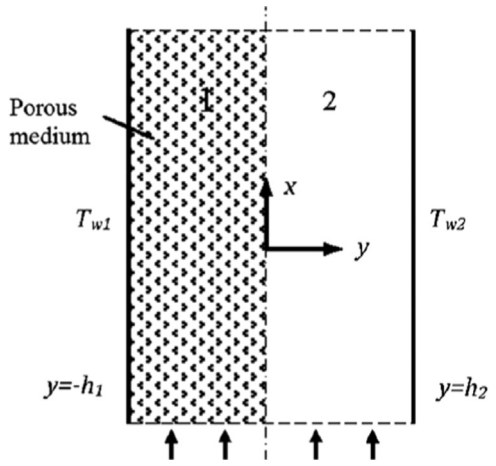

Fig. 34. Schematic diagram of the channel of Hajipour and Dehkordi [104].

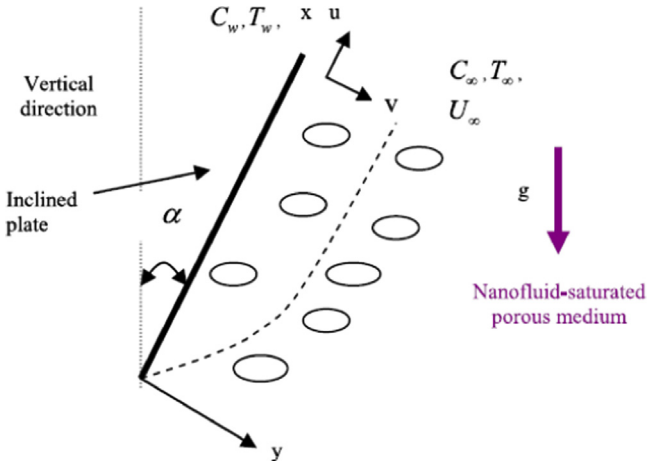

Fig. 36. Physical model and coordinate system of Rana et al. [106].

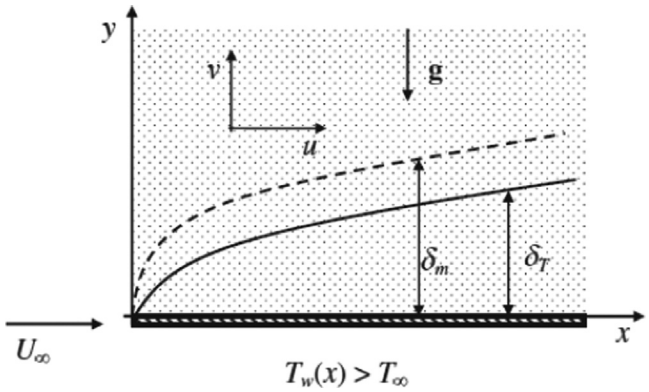

Fig. 35. Physical model and coordinate system of Rosca et al. [105].

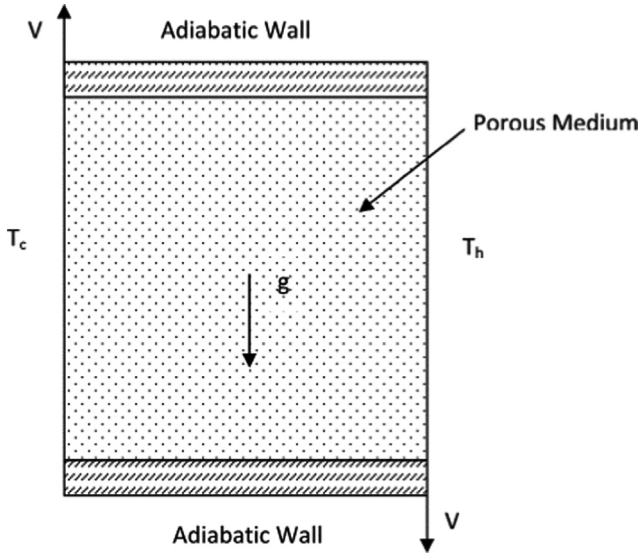

Fig. 37. Schematic diagram of the flow configuration of Mittal et al. [108].

Rosca et al. [105] studied numerically the steady mixed convection boundary layer flow over an impermeable horizontal flat plate embedded in a porous media filled with a nanofluid as shown in Fig. 35. The effect of the volume fraction parameter on Nusselt number was investigated. Their findings indicated that the Nusselt number increased when volume fraction increased.

Rana et al. [106] studied numerically the steady mixed convection boundary layer flow of an incompressible nanofluid along a plate inclined at an angle α in a porous media as shown in Fig. 36. The effects of the Brownian motion and thermophoresis numbers on heat transfer were investigated. Their findings indicated that the Nusselt number decreased with increase in thermophoresis number or Brownian motion number.

Rohni et al. [107] studied numerically the steady mixed convection boundary layer flow on a vertical circular cylinder embedded in a porous media saturated by a nanofluid with both cases of a cooled and heated cylinder. The effects of mixed convection parameter, nanoparticle volume fraction and curvature parameter were investigated. Their findings indicated that when the nanoparticle volume fraction increased, the values of mixed convection heat transfer increased.

Mittal et al. [108] studied numerically the mixed convection in a lid-driven porous cavity saturated by nanofluid as shown in Fig. 37. The effects of Darcy number, Grashof number and volume fraction on the isotherms and the streamlines were studied. Their findings indicated that the addition of nanoparticles to a base fluid had produced an augmentation of the heat transfer coefficient and it was found to increase significantly with an increase of the particle volume concentration. At constant volume fraction and higher value of the Grashof number, with an increase in the Darcy number, the average Nusselt number increased.

Rashad et al. [109] studied numerically the laminar, mixed convection flow of a non-Newtonian fluid past a preamble vertical flat plate embedded in a porous medium saturated with a nanofluid. The influence of the various physical parameters on the velocity, temperature and nanoparticle volume fraction profiles as well as the local Nusselt and Sherwood numbers was investigated. Their findings indicated that the buoyancy ratio increased, both the local Nusselt and Sherwood numbers increased in the entire range of free and mixed convection regimes while they remained constant for the forced-convection regime.

Tham and Nazar [110] studied numerically the steady mixed convection boundary layer flow about a solid sphere with a constant surface temperature and embedded in a porous media filled with a nanofluid. The effects of the Darcy–Brinkman parameter and mixed convection parameter on local Nusselt and Sherwood numbers, skin friction coefficient, velocity and temperature profiles and nanoparticle volume fraction profile were investigated. The results showed that the boundary layer separated from the sphere for some negative values of the mixed convection parameter (opposing flow). Increasing the mixed convection parameter delayed the boundary layer separation and the

separation was completely suppressed for sufficiently large values of the mixed convection parameter.

Mahdi et al. [111] studied numerically the mixed convection heat transfer and fluid flow through various open cell aluminum foams around circular heat source shapes with constant temperature inside a rectangular horizontal channel, filled with nanofluid as shown in Fig. 38. The effects of aluminum foam angle, nanofluid properties and Richardson number on the mixed convection were investigated. The results showed that higher average Nusselt number is obtained with the use of nanofluid and 40PPI aluminum foam pore density with rectangular model. Average Nusselt number with aluminum foam angle decreased with increase in aluminum pore density. Average Nusselt number increased with nanoparticle volume fraction and the mixed convection parameter increased. Higher mixed convection is obtained with the use of aluminum foam angle $\gamma=73.3^{\circ}$.

Amrei and Dehkordi [112] studied the mixed-convection in vertical porous and regular channels for both regular fluids and nanofluids which were been solved using the CFD technique in the entrance regions of momentum and heat transfer taking into account the influences of viscous heating and inertial force. The influences of the Grashof number value on the temperature and velocity distributions in the entrance and fully-developed regions were examined carefully. In addition, temperature and velocity distributions of nanofluids and regular fluids in porous and regular channels were compared.

Mahdi et al. [113] studied numerically the mixed convection heat transfer and fluid flow through an open-cell aluminum foam around various heat source shapes with constant heat flux inside a rectangular horizontal channel, filled with nanofluid as shown in Fig. 39. The effects of aluminum foam, nanofluid properties and Reynolds number on the Nusselt number and friction factor values, with four models in a rectangular horizontal channel, were investigated. The results showed that higher average Nusselt number is obtained with the use of nanofluid (water+SiO_2) and 40PPI aluminum foam pore density at higher Reynolds number with triangular model. Low friction factor is obtained with the use of nanofluid (water+SiO_2) and 10PPI aluminum foam pore density at higher Reynolds number with triangular model. Average Nusselt number increases and friction factor decreases when Reynolds number value increases with all models.

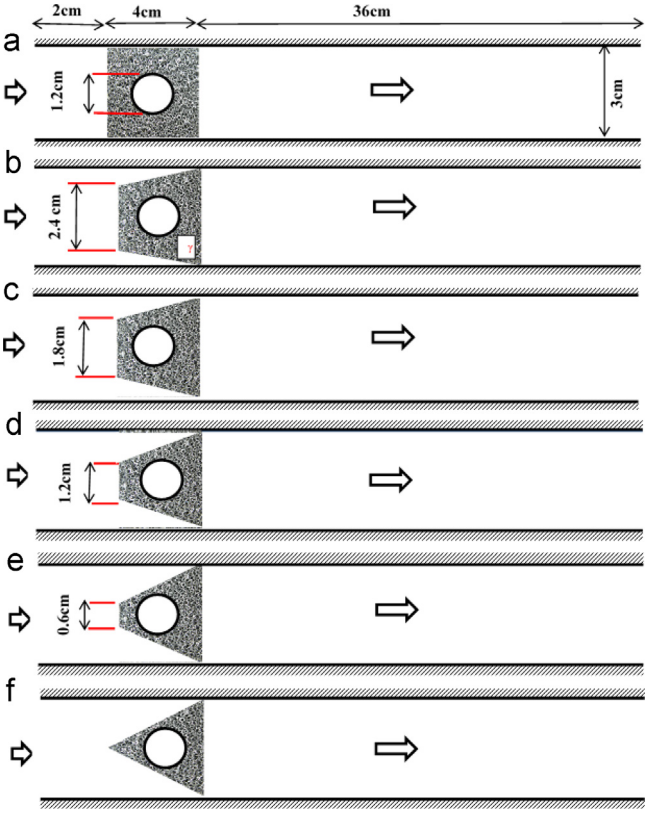

Fig. 38. Physical model and coordinate system of Mahdi et al. [111].

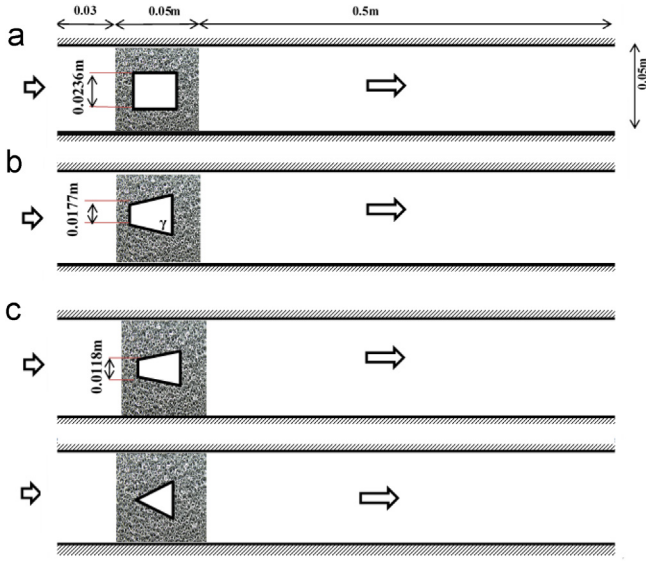

Fig. 39. Physical model and coordinate system of Mahdi et al. [113].

6. Conclusion

Evidently, porous media with nanofluid is highly suited for the application in practical heat transfer processes since it has a great potential for heat transfer enhancement. An opportunity is offered for engineers for developing highly compact and effective heat transfer equipment. A review of previous efforts for different convective flow regimes and heat transfer through porous media with nanofluid is presented in this article.

The effects of several parameters in porous media geometry and thermophysical properties of nanofluid, thermal boundary conditions and types of nanofluids were investigated. Previous studies showed that the convection heat transfer increased with porous media because of its thermal conductivity and thus improved the effective thermal conductivity, leading to a significant increase in convection heat transfer coefficient. Also previous studies showed that the convection heat transfer increased with porous media filled with nanofluids that had high thermal conductivity and this increase depended on nanofluid type.

References

[1] Kreith F, et al. Heat and mass transfer. mechanical engineering handbook. Boca Raton: CRC Press LLC; 1999.
[2] Sparrow E, Grannis V. Pressure drop characteristics of heat exchangers consisting of arrays of diamond-shaped pin fins. Int J Heat Mass Transf 1991;34:589–600.
[3] Chen Z, Li Q, Meier D, Warnecke H. Convective heat transfer and pressure loss in rectangular ducts with drop-shaped pin fins. Heat Mass Transf 1997;33:219–24.
[4] Yun J, Lee K. Investigation of heat transfer characteristics on various kinds of fin-and-tube heat exchangers with interrupted surfaces. Int J Heat Mass Transf 1999;42:2375–85.
[5] Lee K, Kim W, Si J. Optimal shape and arrangement of staggered pins in the channel of a plate heat exchanger. Int J Heat Mass Transf 2001;44:3223–31.
[6] Tanda G. Heat transfer and pressure drop in a channel with diamond-shaped elements. Int J Heat Mass Transf 2001;44:3529–41.

[7] Matos R, Varges J, Laursen T, Bejan A. Optimally staggered finned circular and elliptic tubes in forced convection. Int J Heat Mass Transf 2004;47:1347–59.
[8] Wongwises S, Chokeman Y. Effect of fin pitch and number of tube rows on the air side performance of herringbone wavy fine and tube heat exchangers. Energy Convers Manag 2005;46:2216–31.
[9] Nield D, Bejan A. Convection in porous media. 3rd ed. New York: Springer; 2006.
[10] Das K, Choi U, Yu W, Pradep T. Nanofluid science and technology. USA: Wiley; 2007.
[11] ⟨http://en.wikipedia.org/wiki/Darcy_law⟩ [retrieved 26.12.11].
[12] Oosthuizen PH, Oosthuizen PH, Naylor D. Introduction to convective heat transfer analysis. New York: McGraw Hill; 1998.
[13] Boomsma K, Poulikakos D. On the effective thermal conductivity of a three dimensionally structured fluid-saturated metal foam. Int J Heat Mass Transf 2001;44:827–36.
[14] Bonnet JB, Topin F, Tadrist L. Flow laws in metal foams: compressibility and pore size effects. Transp Porous Media 2008;73(2):233–54.
[15] Boomsma K, Poulikakos D. The effects of compression and pore size variations on the liquid flow characteristics in metal foams. ASME J Fluid Eng 2002;124:263–72.
[16] Bhattacharya A, Calmidi V, Mahajan R. Thermophysical properties of high porosity metal foams. Int J Heat Mass Transf 2002;45:1017–31.
[17] Kleinstreuer C. Modern fluid dynamics-basic theory and selected applications in macro- and micro-fluidics. Springer; 2010.
[18] Jiang P, Wang Z, Ren Z, Wang B. Experimental research of fluid flow and convection heat transfer in plate channels filled with glass or metallic particles. Exp Therm Fluid Sci 1999;20:45–54.
[19] Fu W, Huang H, Liou W. Thermal enhancement in laminar channel flow with a porous block. Int J Heat Mass Transf 1996;39:2165–75.
[20] Boomsma K, Poulikakos D, Zwick F. Metal foams as compact high performance heat exchangers. Mech Mater 2003;35:1161–76.
[21] Jiang P, Li M, Lu T, Yu L, Ren Z. Experimental research on convection heat transfer in sintered porous plate channels. Int J Heat Mass Transf 2004;47:2085–96.
[22] Kaviany M. Principles of heat transfer in porous media. 2nd ed. New York: Springer; 1995.
[23] Caudle B. Introduction to reservoir engineering: steady state flow in porous media. Soc Pet Eng AIME 1976.
[24] Calmidi V. Transport phenomena in high porosity fibrous metal foams. (PhD thesis). University of Colorado; 1998.
[25] Zhao C, Kim T, Lu T, Hodson H. Thermal transport phenomena in porvair metal foams and sintered beds. Micromechanics Centre & Whittle Lab Department of Engineering University of Cambridge; 2001 (Final report).
[26] Plessis P, Montillet A, Comiti J, Legrand J. Pressure drop prediction for flow through high porosity metallic foams. Chem Eng Sci 1994;49:3545–53.
[27] Jiang P, Lu X. Numerical simulation of fluid flow and convection heat transfer in sintered porous plate channels. Int J Heat Mass Transf 2006;49:1685–95.
[28] Ergun S. Fluid flow through packed columns. Chem Eng Prog 1952;48:89–94 (available)⟨http://legacy.library.ucsf.edu/documentStore/e/f/k/efk76a99/Sefk76a99.pdf⟩.
[29] Nebbali R, Bouhadef K. Non-Newtonian fluid flow in plane channels: heat transfer enhancement using porous blocks. Int J Therm Sci 2011;50:1984–95.
[30] Christopher RH, Middleman S. Power-law flow through a packed tube. Ind Eng Chem Fundam 1965;4:422–6.
[31] Givler R, Altobelli S. A determination of the effective viscosity for the Brinkmann-Forchheimer flow model. J Fluids Eng 1994;258:355–70.
[32] Ansys 14.0 Help. FLUENT User's Guide, Release 14.0 2011; SAS IP, Inc.
[33] Antohe B, Lage J. Experimental determination of permeability and inertia coefficients of mechanically compressed aluminium porous matrices. ASME J Fluid Eng 1997;119:404–12.
[34] Calmidi V, Mahajan R. the effective thermal conductivity of high porosity metal foams. ASME J Heat Transf 1999;121:466–71.
[35] Phanikumar M, Mahajan L. Non-Darcy natural convection in high porosity metal foams. Int J Heat Mass Transf 2002;45:3781–93.
[36] Hadim H, North M. Forced convection in a sintered porous channel with inlet and outlet slots. Int J Therm Sci 2005;44:33–42.
[37] Hunt M, Tien C. Effects of thermal dispersion on forced convection in fibrous media. Int J Heat Mass Transf 1988;31:301–9.
[38] Cheng P, Hsu C, Chowdhury A. Forced convection in the entrance region of a packed channel with asymmetric heating. ASME J Heat Transf 1988;110:946–54.
[39] Wakao N, Kaguei S. Heat and mass transfer in packed beds. New York: Gordon and Breach, London Science Publishers; 1982.
[40] Zehener P. Waermeleitfahigkeit won Schuettungen be Massigen Temperaturea. Chem.-Ingr.-Tech 1970;42:933–41.
[41] Massoud M. Engineering thermo-fluids. Berlin Heidelberg: Springer-Verlag; 2005.
[42] Wang X, Mujumdar A. Heat transfer characteristics of nanofluids: a review. Int J Therm Sci 2007;46:1–19.
[43] Yu W, France DM, Routbort JL, Choi SUS. Review and comparison of nanofluid thermal conductivity and heat transfer enhancements. Heat Transf Eng 2008;29:432–60.
[44] Nic M, Jirat J, Kosata B, ⟨http://en.wikipedia.org/wiki/Volume_fraction⟩; 2006.
[45] Karthikeyan N, Philip J, Raj B. Effect of clustering on the thermal conductivity of nanofluids. Mater Chem Phys 2008;109:50–5.
[46] Jang S, Choi S. Role of Brownian motion in the enhanced thermal conductivity of nanofluids. Appl Phys Lett 2004;84:4316.
[47] Singh A. Thermal conductivity of nanofluids. Review paper. Def Sci J 2008;58:600–7.
[48] Chen C, Ding C. Study on the thermal behavior and cooling performance of a nanofluid-cooled micro-channel heat sink. Int J Therm Sci 2011;50:378–84.
[49] Vajjha R, Das D, Mahagaonkar B. Density measurements of different nanofluids and their comparison with theory. Pet Sci Technol 2009;27:612–24.
[50] Pak B, Cho Y. Hydrodynamic and heat transfer study of dispersed fluids with submicron metallic oxide particles. Exp Heat Transf 1998;11:151–70.
[51] Corcione M. Heat transfer features of buoyancy-driven nanofluids inside rectangular enclosures differentially heated at the sidewalls. Int J Therm Sci 2010;49:1536–46.
[52] Abu-Nada E, Oztop HF, Pop I. Buoyancy induced flow in a nanofluid filled enclosure partially exposed to forced convection. Superlattices Microstruct 2012;51:381–95.
[53] Xuan Y, Roetzel W. Conceptions for heat transfer correlations of nanofluids. Int J Heat Mass Transf 2000;43:3701–7.
[54] Chon C, Kim K, Lee S, Choi S. Empirical correlation finding the role of temperature and particle size for nanofluid (Al_2O_3) thermal conductivity enhancement. Appl Phys Lett 2005;87:153107.
[55] Li C, Peterson G. Experimental investigation of temperature and volume fraction variations on the effective thermal conductivity of nanoparticle suspensions (nanofluids). J Appl Phys 2006;99:084314.
[56] Masuda H, Ebata A, Teramae K, Hishinuma N. Alteration of thermal conductivity and viscosity of liquid by dispersing ultra-fine particles (dispersion of γ-Al_2O_3, SiO_2, and TiO_2 ultra-fine particles). Netsu Bussei (Japan) 1993;4:227–33.
[57] Özerinç S, Kakaç S, Yazıcıoğlu A. Enhanced thermal conductivity of nanofluids: a state-of-the-art review. Microfluid Nanofluidics 2010;8:145–70.
[58] Wang X, Mujumdar A. A review on nanofluids-part I: theoretical and numerical investigations. Braz J Chem Eng 2008;25:613–30.
[59] Maxwell J. A treatise on electricity and magnetism. 3rd ed. Oxford, UK: Clarendon Press; 1873.
[60] Einstein A. A new determination of molecular dimensions. Wiley Online Library, Annalen der Physik ; 1906. 4: 289–306. Available from: ⟨http://www.ffn.ub.es/luisnavarro/nuevo_maletin/Einstein_1906_thesis.pdf⟩.
[61] Koo J, Kleinstreuer C. A new thermal conductivity model for nanofluids. J Nanoparticle Res 2004;6:577–88.
[62] Xu J, Yu B, Zou M, Xu P. A new model for heat conduction of nanofluids based on fractal distributions of nanoparticles. J Phys D: Appl Phys 2006;39:4486–90.
[63] Xuan Y, Li Q, Hu W. Aggregation structure and thermal conductivity of nanofluids. Gen Introd Chem Eng, Am Inst Chem Eng (AIChE) J 2003;49:1038–43.
[64] Prasher R, Phelan P, Bhattacharya P. Effect of aggregation kinetics on the thermal conductivity of nanoscale colloidal solutions (nanofluid). Am Chem Soc, Nano Lett 2006;6:1529–34.
[65] Yu W, Choi S. The role of interfacial layers in the enhanced thermal conductivity of nanofluids: a renovated Maxwell Model. J Nanoparticle Res 2003;5:167–71.
[66] Maïga S, Nguyen C, Galanis N, Roy G. Heat transfer behaviours of nanofluids in a uniformly heated tube. Superlattices Microstruct 2004;35:543–57.
[67] Koo J, Kleinstreuer C. Laminar nanofluid in micro-heat sinks. Int J Heat Mass Transf 2005;48:2652–61.
[68] He Y, Men Y, Zhao Y, Lu H, Ding Y. Numerical investigation in to the convective heat transfer of TiO_2 nanofluids flowing through a straight tube under the laminar flow conditions. Appl Therm Eng 2009;29:1965–72.
[69] Nield D, Kuznetsov A. Thermal instability in a porous medium layer saturated by a nanofluid. Int J Heat Mass Transf 2009;52:5796–801.
[70] Kuznetsov A, Nield D. Natural convective boundary-layer flow of a nanofluid past a vertical plate. Int J Therm Sci 2010;49:243–7.
[71] Sun Q, Pop I. Free convection in a triangle cavity filled with a porous medium saturated with nanofluids with flush mounted heater on the wall. Int J Therm Sci 2011;50:2141–53.
[72] Chamkha A, Gorla R, Ghodeswar K. Non-similar solution for natural convective boundary layer flow over a sphere embedded in a porous medium saturated with a nanofluid. Transp Porous Media 2011;86:13–22.
[73] Rashad A, EL-Hakiem M, Abdou M. Natural convection boundary layer of a non-Newtonian fluid about a permeable vertical cone embedded in a porous medium saturated with a nanofluid. Comput Math Appl 2011;62:3140–51.
[74] Hady F, Ibrahim F, Abdel-Gaied S, Eid M. Effect of heat generation/absorption on natural convective boundary-layer flow from a vertical cone embedded in a porous medium filled with a non-Newtonian nanofluid. Int Commun Heat Mass Transf 2011;38:1414–20.
[75] Nield D, Kuznetsov A. The Cheng Minkowycz problem for the double diffusive natural convective boundary layer flow in a porous medium saturated with a nanofluid. Int J Heat Mass Transf 2011;54:374–8.
[76] Cheng P, Minkowycz W. Free convection about a vertical flat plate embedded in a porous medium with application to heat transfer from a dike. J Geophys Res 1977;82:2040–4.
[77] Kuznetsov A, Nield D. Double-diffusive natural convective boundary-layer flow of a nanofluid past a vertical plate. Int J Therm Sci 2011;50:712–7.
[78] Bhadauria B, Agarwal S, Kumar A. Nonlinear two-dimensional convection in a nanofluid saturated porous medium. Transp Porous Media 2011;90:605–25.

[79] Hady F, Ibrahim F, Abdel-Gaied S, Eid M. Influence of yield stress on free convective boundary-layer flow of a non-Newtonian nanofluid past a vertical plate in a porous medium. J Mech Sci Technol 2011;25:2043–50.
[80] Khan W, Aziz A. Double-diffusive natural convective boundary layer flow in a porous medium saturated with a nanofluid over a vertical plate: prescribed surface heat, solute and nanoparticle fluxes. Int J Therm Sci 2011;50: 2154–60.
[81] Aziz A, Khan W, Pop I. Free convection boundary layer flow past a horizontal flat plate embedded in porous medium filled by nanofluid containing gyrotactic microorganisms. Int J Therm Sci 2012;56:48–57.
[82] Agarwal S, Sacheti NC, Chandran P, Bhadauria BS, Singh AK. Non-linear convective transport in a binary nanofluid saturated porous layer. Transp Porous Media 2012;93:29–49.
[83] Cheng C. Natural convection boundary layer flow over a truncated cone in a porous medium saturated by a nanofluid. Int Commun Heat Mass Transf 2012;39:231–5.
[84] Mahdy A, Ahmed S. Laminar free convection over a vertical wavy surface embedded in a porous medium saturated with a nanofluid. Transp Porous Media 2012;91:423–35.
[85] Yadav D, Bhargava R, Agrawal G. Boundary and internal heat source effects on the onset of Darcy-Brinkman convection in a porous layer saturated by nanofluid. Int J Therm Sci 2012;60:244–54.
[86] Cheng C. Free convection boundary layer flow over a horizontal cylinder of elliptic cross section in porous media saturated by a nanofluid. Int Commun Heat Mass Transf 2012;39:931–6.
[87] Chand R, Rana G. On the onset of thermal convection in rotating nanofluid layer saturating a Darcy-Brinkman porous medium. Int J Heat Mass Transf 2012;55:5417–24.
[88] Uddin MJ, Khan WA, Ismail AIM. Free convection boundary layer flow from a heated upward facing horizontal flat plate embedded in a porous medium filled by a nanofluid with convective boundary condition. Transp Porous Media 2012;92:867–81.
[89] Chand R, Rana GC. Oscillating convection of nanofluid in porous medium. Transp Porous Media 2012;95:269–84.
[90] Chamkha AJ, Ismael MA. Conjugate heat transfer in a porous cavity filled with nanofluids and heated by a triangular thick wall. Int J Therm Sci 2013;67:135–51.
[91] Khan WA, Uddin MJ, Ismail AIM. Free convection of non-Newtonian nanofluids in porous media with gyrotactic microorganisms. Transp Porous Media 2013;97:241–52.
[92] Umavathi JC, Mohite MB. The onset of convection in a nanofluid saturated porous layer using Darcy model with cross diffusion. Meccanica 2014;49: 1159–75.
[93] Ghazvini M, Shokouhmand H. Investigation of a nanofluid-cooled microchannel heat sink using fin and porous media approaches. Energy Convers Manag 2009;50:2373–80.
[94] Bachok N, Ishak A, Pop I. Flow and heat transfer over a rotating porous disk in a nanofluid. Phys B: Condens Matter 2011;406:1767–72.
[95] Das K. Slip flow and convective heat transfer of nanofluids over a permeable stretching surface. Comput Fluids 2012;64:34–42.
[96] Maghrebi M, Nazari M, Armaghani T. Forced convection heat transfer of nanofluids in a porous channel. Transp Porous Media 2012;93:401–13.
[97] Servati Ata AV, Javaherdeh K, Ashorynejad HR. Magnetic field effects on force convection flow of a nanofluid in a channel partially filled with porous media using Lattice Boltzmann method. Adv Powder Technol 2014;25:666–75.
[98] Hosseini M, Mohammadian E, Shirvani M, Mirzababaei SN, Aski F Shakeri. Thermal analysis of rotating system with porous plate using nanofluid. Powder Technol 2014;254:563–71.
[99] Hatami M, Heikholeslami MS, Ganji DD. Laminar flow and heat transfer of nanofluid between contracting and rotating disks by least square method. Powder Technol 2014;253:769–79.
[100] Ahmad S, Pop I. Mixed convection boundary layer flow from a vertical flat plate embedded in a porous medium filled with nanofluids. Int Commun Heat Mass Transf 2010;37:987–91.
[101] Nazar R, Tham L, Pop I, Ingham D. Mixed convection boundary layer flow from a horizontal circular cylinder embedded in a porous medium filled with a nanofluid. Transp Porous Media 2011;86:517–36.
[102] Gorla R, Chamkha A, Rashad A. Mixed convective boundary layer flow over a vertical wedge embedded in a porous medium saturated with a nanofluid: natural convection dominated regime. Nanoscale Res Lett 2011;6:207.
[103] Cimpean D, Pop I. Fully developed mixed convection flow of a nanofluid through an inclined channel filled with a porous medium. Int J Heat Mass Transf 2012;55:907–14.
[104] Hajipour M, Dehkordi A. Analysis of nanofluid heat transfer in parallel-plate vertical channels partially filled with porous medium. Int J Therm Sci 2012;55:103–13.
[105] Rosca A, Rosca N, Grosan T, Pop I. Non-Darcy mixed convection from a horizontal plate embedded in a nanofluid saturated porous media. Int Commun Heat Mass Transf 2012;39:1080–5.
[106] Rana P, Bhargava R, Bég O. Numerical solution for mixed convection boundary layer flow of a nanofluid along an inclined plate embedded in a porous medium. Comput Math Appl 2012;64:2816–32.
[107] Rohni AM, Ahmad S, Merkin JH, Pop I. Mixed convection boundary-layer flow along a vertical cylinder embedded in a porous medium filled by a nanofluid. Transp Porous Media 2013;96:237–53.
[108] Mittal N, Manoj V, Kumar D, Satheesh A. Numerical simulation of mixed convection in a porous medium filled with water/Al_2O_3 nanofluid. Heat Transf—Asian Res 2013;42:1.
[109] Rashad A, Chamkha A, Abdou M. Mixed convection flow of non-Newtonian fluid from vertical surface saturated in a porous medium filled with a nanofluid. JAFM, J Appl Fluid Mech 2013;6:301–9.
[110] Tham L, Nazar R. Numerical solution of mixed convection flow about a sphere in a porous medium saturated by a nanofluid: Brinkman model. J Sci Technol 2012;4:35–46.
[111] Mahdi RA, Mohammed HA, Munisamy KM. The effect of various open cell aluminium foam geometrical shapes on combined convection heat transfer with nanofluid. Int J Emerg Technol Adv Eng 2013;3:615–29.
[112] Amrei Hashemi SMH, Dehkordi AM. Modeling and CFD simulation of a mixed-convection flow of regular fluids and nanofluids in vertical porous and regular channels. Heat Transf—Asian Res 2014;43:243–69.
[113] Mahdi RA, Mohammed HA, Munisamy KM, Saeid NH. Influence of various geometrical shapes on mixed convection through an open-cell aluminium foam filled with nanofluid. J Comput Theor Nanosci 2014;11: 1275–89.